Journal of Wind Engineering & Industrial Aerodynamics 255 (2024) 105937

Contents lists available at ScienceDirect

Journal of Wind Engineering & Industrial Aerodynamics

journal homepage: www.elsevier.com/locate/jweia

# Time-domain state-space model formulation of motion-induced aerodynamic forces on bridge decks

Simian Lei [a,b], Luca Patruno [b,*], Claudio Mannini [c], Stefano de Miranda [b], Yaojun Ge [a]

[a] Department of Bridge Engineering, Tongji University, Shanghai, China
[b] Department of Civil, Chemical, Environmental, and Materials Engineering, University of Bologna, Bologna, Italy
[c] Department of Civil and Environmental Engineering, University of Florence, Florence, Italy

ARTICLE INFO

*Keywords:*
Motion-induced forces
State-space model
Indicial function
Unsteady aerodynamics
Bridge aerodynamics

ABSTRACT

Motion-induced aerodynamic forces play a fundamental role in the stability and buffeting analysis of long-span bridges, which are traditionally performed in the frequency domain adopting the well-known approach based on flutter derivatives and aerodynamic admittance functions. However, the increase in span of newly designed bridges currently raises concerns regarding the role of nonlinear aerodynamic effects, the response to non-stationary winds and the aerodynamic coupling in multi-modal vibrations. Addressing these issues requires to calculate aerodynamic forces induced by arbitrary motions and, possibly, consider large variations in the incoming flow orientation, a task better suited for time-domain approaches. In this study, we introduce a time-domain state-space model formulation for motion-induced aerodynamic forces, which systematizes and generalizes previous models, while keeping a simple structure and ease of calibration. We tailor the model formulation to allow for a clear distinction between quasi-static and purely transient aerodynamic contributions and investigate the relations between the proposed model and other available models, highlighting their common underlying framework. The model is finally calibrated for a selection of bridge decks, showing a very good ability to reproduce motion-induced aerodynamic forces.

## 1. Introduction

Modeling of wind-induced forces on bridge deck sections is of fundamental importance for the assessment of flutter stability, as well as the evaluation of buffeting response of long-span bridges (Diana et al., 2023). In particular, as it is well known, both motion-induced and gust-induced aerodynamic loads are characterized by delay effects (and potential overshoots) with respect to forces measured in static conditions at the same angle of attack, importantly limiting the accuracy attainable by pure quasi-steady formulations (Chen et al., 2000a; Diana et al., 2008). As a result, in current engineering practice, aeroelastic stability analyses are conducted in the frequency-domain relying on the evaluation of flutter derivatives, which represent the Frequency Response Functions, FRF, between the bridge-deck section motions and the produced aerodynamic forces (Theodorsen, 1949; Scanlan, 1993). Similarly, as regard gust-induced forces, the approach usually adopted requires to evaluate aerodynamic admittance functions, representing the module of the FRF between incoming velocity fluctuations and corresponding aerodynamic forces (Sears, 1941; Scanlan, 1993). Both approaches linearize the aeroelastic behavior in the proximity of a reference angle of attack, disregarding aerodynamic nonlinearities, which are then considered by checking the result sensitivity with respect to the angle used for linearization. However, the necessity to consider the nonlinearity of the aerodynamic behavior at moderate to large angles of attack conflicts with the adoption of FRF-based models which, in turn, are well-adapted for the representation of fluid-memory effects (Wu and Kareem, 2013). In addition, the non-stationary nature of the excitation caused by non-synoptic winds shall be considered, which makes time-domain approaches natural candidates for their analysis (Calamelli et al., 2024).

To solve the problem, starting from the plain Quasi-Steady, QS, formulation, valid at high reduced velocities, the simplest improvement is represented by the introduction of deck angular velocity in the effective angle of attack (see, for instance, Van Oudheusden (1995)). Indeed, the introduction of such term allows the QS theory to account for the presence of aerodynamic damping in the rotational degree of freedom, which would be otherwise completely disregarded. However, as stated by Van Oudheusden (1995) "[...] Attempts have been made to model the rotation by using a characteristic relative velocity to approximate the averaged flow field [...] in analogy of the use of the three-quarter chord point in airfoil flutter. There is however no

* Corresponding author.
*E-mail address:* luca.patruno@unibo.it (L. Patruno).

https://doi.org/10.1016/j.jweia.2024.105937
Received 2 August 2024; Received in revised form 12 October 2024; Accepted 27 October 2024
Available online 9 November 2024
0167-6105/© 2024 The Authors. Published by Elsevier Ltd. This is an open access article under the CC BY license (http://creativecommons.org/licenses/by/4.0/).

justification for this in the case of separated flow, and this prevents the use of a simple, rigorous quasi-steady theory [...]". Nevertheless, the introduction of such a term is necessary to comply with the results analytically derived for the airfoil theory and experimentally obtained for bridge decks.

Numerous further enrichments of the QS theory have been proposed in the literature and the Reader is invited to refer to Wu and Kareem (2013) for a review. Notable examples of such approaches are the quasi-static corrected theory proposed by Diana et al. (1993), those based on Rheological Models, RMs, Diana et al. (2008, 2010, 2013) and Diana and Omarini (2020) and those based on Rational Function Approximation, RFA, of the measured FRF (Chen et al., 2000b; Chen and Kareem, 2001, 2003; Barni et al., 2021, 2022). In these models, the aerodynamic forcing (i.e., deck motion and/or incoming gusts) can be split into a low-frequency and a high-frequency component (band-superposition approach). The first contribution is responsible for the nonlinear modulation of self-excited forces and can be dealt with in a quasi-steady sense. For the second contribution, a State-Space Model, SSM, whose coefficients can depend on the low-frequency effective angle of attack, is adopted (Diana et al., 2013; Barni et al., 2021). RFA models are built by approximating the measured aerodynamic FRF (i.e., flutter derivatives) according to the technique described in Roger (1977) and Caracoglia and Jones (2003). A detailed discussion of RFA and some interesting extensions of the original technique can be found in Øiseth et al. (2011). In contrast, RMs are deduced exploiting the similarity between constitutive relations used for hysteretic materials and relations occurring between aerodynamic excitations and corresponding forces. It must be noted that, in both cases, the SSM is deduced assuming particular forms *a priori*, having as main target an accurate reproduction of the measured flutter derivatives.

Other approaches have also been followed to deal with aerodynamic nonlinearities. Wu and Kareem (2011) proposed a black-box model based on a cellular automata nested neural network, while Wu and Kareem (2014) set up a sparse third-order single-input single-output Volterra model. The latter can be considered a gray-box model as the Volterra kernels are pruned, reducing the high computational cost of the model, based on some aerodynamic considerations. A nonlinear model for buffeting and self-excited forces to be used in combination with a finite-element model of a bridge is that proposed by Zhou et al. (2018). The model is very general but seemingly not so easy to identify and interpret due to the large number of parameters. A few models have also been proposed to consider the nonlinear dependence of self-excited forces on vibration amplitude, mainly aiming at predicting postcritical flutter limit-cycle oscillations (e.g., Náprstek et al. (2007), Král et al. (2014) and Gao et al. (2020)).

In this paper, after summarizing the main results of thin-airfoil theory, we propose a general framework for the representation of unsteady aerodynamic loads in the time domain. In particular, inspired by thin-airfoil theory, the evolution of aerodynamic coefficients is represented by a state-space model, whose forcing term accounts for the variation in deck orientation with respect to the incoming flow. Attention is put in carefully splitting quasi-static contributions from purely transient terms, a feature which is particularly desirable for a straightforward extension of the model to nonlinear cases. The FRF associated with the proposed model is rigorously deduced, allowing one to drive the model calibration relying on measured flutter derivatives. The resulting model appears to be simple yet general, and the study of its interrelations with other models available in the literature provides a comprehensive perspective on the use of SSM for the modeling of motion-induced aerodynamic forces.

The paper is organized as follows. In Section 2 the main features of airfoil theory are briefly summarized. In Section 3, the present model is introduced, relating it to the airfoil theory and other models available in the literature, as well as providing details regarding its calibration. In Section 4, the model is calibrated for a selection of bridge deck sections. Finally, in Section 5, conclusions are drawn.

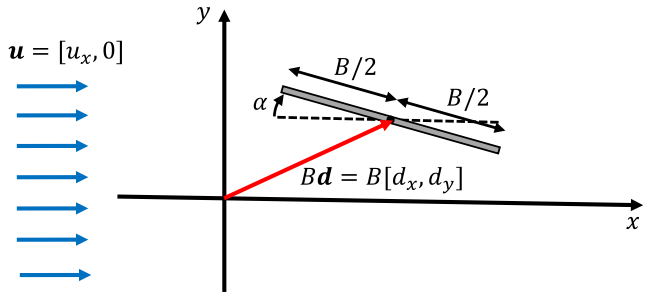


**Fig. 1.** The airfoil: reference system and sign convention.

## 2. Thin-airfoil theory

In this section, we briefly recall the principal results of thin-airfoil theory, mainly useful to set the ground for further developments and present the adopted notation. In particular, we consider the reference system reported in Fig. 1.

The airfoil center is pointed by the non-dimensional displacement vector $\boldsymbol{d} = [d_x, d_y]$, so that it is located at $B\boldsymbol{d}$ from the reference system origin, being $B$ the chord. The incoming wind velocity is denoted as $\boldsymbol{u} = [u_x, u_y]$, but, for the sake of simplicity, we here assume velocity to be directed along $x$, so that $\boldsymbol{u} = [u_x, 0] = [U, 0]$, where $U$ is the velocity magnitude. Angles are measured according to the nose-up convention, and we assume $d_x = 0$, as well as small values of $\alpha$. In such conditions, at equilibrium, the aerodynamic forces acting on the thin-airfoil can be expressed as

$$F_y = \frac{1}{2}\rho U^2 B\left[C_y^{eq}(0) + C_y'\alpha\right], \qquad M = F_y\frac{B}{4}, \tag{1}$$

where $F_y$ is the aerodynamic force directed in the $y$ direction, $M$ is the aerodynamic pitching moment oriented as $\alpha$ and calculated with respect to the airfoil center, $\rho$ is the fluid density and the lift coefficient, $C_y^{eq}$, has been expanded in a first-order Taylor series. In particular, $C_y^{eq}(\alpha)$ represents the equilibrium (i.e., long-term) value of $C_y$ at the wind angle of attack $\alpha$, while $C_y' = \frac{\mathrm{d}C_y^{eq}}{\mathrm{d}\alpha}$. As it is well known, the lift force is applied at the point located $B/4$ upstream the airfoil mid-chord point. Additionally, $C_y' = 2\pi$ and, for an airfoil with a symmetric profile with respect to the chord line, $C_y^{eq}(0) = 0$. We notice that for real airfoils the adopted first-order approximation of the lift coefficient, as well as the constant value assumed for its application point, remain approximately valid only up to the stall angle (say around 10°). Wagner (1924) showed that it is possible to define an effective angle of attack, $\alpha_{dw}$, usually referred to as the downwash angle, as

$$\alpha_{dw}(s) = \alpha(s) + \frac{1}{4}\dot{\alpha}(s) - \dot{d}_y(s), \tag{2}$$

where the dot denotes differentiation with respect to the non-dimensional time $s = tU/B$ (so that $\mathrm{d}/\mathrm{d}s = B/U\ \mathrm{d}/\mathrm{d}t$). In particular, once equilibrium aerodynamic forces are reached for an angle $\bar{\alpha}$, small sudden variations of the downwash angle, $\mathrm{d}\alpha_{dw}$, lead to

$$F_y(s) = \frac{1}{2}\rho U^2 B\left[C_y^{eq}(\bar{\alpha}) + \mathrm{d}\alpha_{dw}\ C_y'\phi(s) + \frac{\pi}{2}\dot{\alpha} - \frac{\pi}{2}\ddot{d}_y\right], \tag{3}$$

being $\phi(s)$ the Wagner function and analogously

$$M(s) = \frac{1}{2}\rho U^2 B^2\left[C_m^{eq}(\bar{\alpha}) + \mathrm{d}\alpha_{dw}\ C_m'\phi(s) - \frac{\pi}{8}\dot{\alpha} - \frac{\pi}{64}\ddot{\alpha}\right], \tag{4}$$

where $C_m^{eq}(\bar{\alpha}) = \frac{1}{4}C_y^{eq}(\bar{\alpha})$, $C_m'/C_y' = 1/4$. The first two terms of Eqs. (3) and (4) are usually denoted as circulatory contributions, while the others, expressed in terms of time derivatives of $\alpha$ and $d_y$, are of non-circulatory nature. The Wagner function $\phi(s)$, represents the time evolution of the aerodynamic forces due to a unit step change in the effective angle of attack (i.e., the indicial response), and, as it is well known, it can be used in a Duhamel's integral in order to calculate the

aerodynamic forces arising due to arbitrary motions (Scanlan, 1993). Often, the Wagner function is approximated as proposed by Jones (1940)

$$\phi(s) = 1 - 0.165e^{-0.091s} - 0.335e^{-0.6s}. \tag{5}$$

Analogously, as shown by Theodorsen (1949), it is possible to consider small constant-amplitude sinusoidal oscillations of the type

$$d_y(K,s) = \tilde{d}_y e^{iKs}, \qquad \alpha(K,s) = \bar{\alpha} + \tilde{\alpha} e^{iKs}, \tag{6}$$

where $i$ is the imaginary unit, $\tilde{d}_y$ and $\tilde{\alpha}$ are complex amplitudes, $\bar{\alpha}$ is the mean angle of attack around which the airfoil oscillates, and $K = \Omega B/U$ is a reduced frequency, being $\Omega$ the circular frequency in the dimensional time, so that $Ks = \Omega t$. In such conditions, it is possible to write the downwash angle as

$$\alpha_{dw}(K,s) = \left[\tilde{\alpha}\left(1 + \frac{1}{4}iK\right) - iK\tilde{d}_y\right] e^{iKs}. \tag{7}$$

Then, the aerodynamic lift (complex-valued) can be expressed by means of Theodorsen's circulation function, $C(K)$, as

$$F_y(K,s) = \frac{1}{2}\rho U^2 B\left\{C_y^{eq}(\bar{\alpha}) + \left[C_y' C(K)\tilde{\alpha}_{dw} + \frac{\pi}{2}iK\tilde{\alpha} + \frac{\pi}{2}K^2\tilde{d}_y\right] e^{iKs}\right\}, \tag{8}$$

and, analogously, the aerodynamic pitching moment is

$$M(K,s) = \frac{1}{2}\rho U^2 B^2\left\{C_m^{eq}(\bar{\alpha}) + \left[C_m' C(K)\tilde{\alpha}_{dw} - \frac{\pi}{8}iK\tilde{\alpha} + \frac{\pi}{64}K^2\tilde{\alpha}\right] e^{iKs}\right\}, \tag{9}$$

Theodorsen's circulation function represents the Fourier transform of Wagner's function (Garrick, 1938) and, adopting (Jones, 1940) approximation (see Eq. (5)), can be written as

$$C(K) = 1 - \frac{0.165iK}{iK + 0.091} - \frac{0.335iK}{iK + 0.6}. \tag{10}$$

It is finally possible to rearrange Eqs. (8) and (9) in Scanlan's notation using flutter derivatives (Scanlan, 1993) as

$$F_y(K,s) = \frac{1}{2}\rho U^2 B\left[C_y^{eq}(\bar{\alpha}) + KH_1^*\dot{d}_y + KH_2^*\dot{\alpha} + K^2H_3^*\alpha + K^2H_4^*d_y\right], \tag{11}$$

$$M(K,s) = \frac{1}{2}\rho U^2 B^2\left[C_m^{eq}(\bar{\alpha}) + KA_1^*\dot{d}_y + KA_2^*\dot{\alpha} + K^2A_3^*\alpha + K^2A_4^*d_y\right], \tag{12}$$

where $H_i^* = H_i^*(K)$ and $A_i^* = A_i^*(K)$ are the well-known flutter derivatives, representing the components of the FRF between airfoil motion and aerodynamic forces. In particular, assuming the aerodynamic forces coefficient to be expressed in the form

$$C_y(K,s) = C_y^{eq}(\bar{\alpha}) + \tilde{C}_y e^{iKs}, \qquad C_m(K,s) = C_m^{eq}(\bar{\alpha}) + \tilde{C}_m e^{iKs}, \tag{13}$$

with $\tilde{C}_y$ and $\tilde{C}_m$ complex amplitudes of the aerodynamic coefficients, if $\tilde{d}_y \neq 0$ and $\tilde{\alpha} = 0$, it is possible to write

$$\frac{\tilde{C}_y}{\tilde{d}_y} = (H_4^* + iH_1^*)K^2, \qquad \frac{\tilde{C}_m}{\tilde{d}_y} = (A_4^* + iA_1^*)K^2, \tag{14}$$

while, for $\tilde{d}_y = 0$ and $\tilde{\alpha} \neq 0$

$$\frac{\tilde{C}_y}{\tilde{\alpha}} = (H_3^* + iH_2^*)K^2, \qquad \frac{\tilde{C}_m}{\tilde{\alpha}} = (A_3^* + iA_2^*)K^2. \tag{15}$$

For the sake of conciseness, the Reader is invited to refer to Scanlan (1993) for the expressions of $H_i^*$ and $A_i^*$ in terms of $C(K)$.

As regard the response to incoming periodic gusts, we only recall here that the indicial response for an impinging vertical gust with a sharp edge is Küssner's function, $\psi(s)$ (analogue of Wagner's function), and that its Fourier transform is Sears's function, $S(K)$ (analogue of Theodorsen's function). Küssner's function can be approximated as (Scanlan, 1993)

$$\psi(s) = 1 - 0.5e^{-0.26s} - 0.5e^{-2.0s}, \tag{16}$$

and the corresponding approximation of Sears's function, obtained again by Fourier transformation, is

$$S(K) = \left(1 - \frac{0.5iK}{iK + 0.26} - \frac{0.5iK}{iK + 2.0}\right) e^{iK/2}, \tag{17}$$

where the last term $e^{iK/2}$ is necessary to account for the fact that the growth in the aerodynamic forces starts when the gust impinges the leading edge, i.e. $s = -1/2$, and can be obtained using the Time Translation Theorem of the Fourier transform. A comparison between approximate and exact indicial responses (and the corresponding FRF) to changes in the angle of attack (i.e., Wagner's and Theodorsen's functions) and a sharp incoming vertical gust (i.e., Küssner's and Sears's functions) is provided in Fig. 2, where Sears's function is multiplied by $e^{-iK/2}$ to remove the abovementioned time shift. The strong formal analogy between motion-induced and gust-induced aerodynamic responses for the thin airfoil can clearly be appreciated. The Reader is invited to refer, for instance, to Scanlan (1993), Leishman (2002), Caracoglia and Jones (2003) and Fung (2008) for further details.

## 3. A general state-space model

We reconsider Fig. 1, assuming a stationary wind not aligned with the global $x$-axis and introducing the wind reference system, $D - L$ (aligned with the relative velocity between deck center and surrounding fluid), and the bridge-deck section reference system, $\xi - \eta$, as shown in Fig. 3.

We define the relative velocity between deck center and wind as

$$\boldsymbol{u}_r = \boldsymbol{u} - \frac{\mathrm{d}(\boldsymbol{B}\boldsymbol{d})}{\mathrm{d}t}, \tag{18}$$

and denote the effective angle of attack between fluid and deck as

$$\alpha_e = \alpha + \mathrm{atan}\left(\frac{u_{r,x}}{u_{r,y}}\right) = \alpha + \alpha_{wr}, \tag{19}$$

$\alpha_{wr}$ is the inclination of the relative velocity between deck center and wind in the $x - y$ reference system. We assume the usual expression for aerodynamic forces

$$\boldsymbol{F} = \begin{bmatrix} F_x \\ F_y \\ M \end{bmatrix} = \frac{1}{2}\rho U_r^2 \begin{bmatrix} B\,C_x \\ B\,C_y \\ B^2\,C_m \end{bmatrix} = \frac{1}{2}\rho U_r^2 \boldsymbol{B}\boldsymbol{C}_{a,xy} = q\boldsymbol{B}\boldsymbol{C}_{a,xy}, \tag{20}$$

where $q$ is the dynamic pressure, $\boldsymbol{C}_{a,xy} = [C_x, C_y, C_m]^T$, $U_r$ is the magnitude of the relative velocity vector between fluid and deck center, and $\boldsymbol{B} = \mathrm{diag}([B, B, B^2])$, with diag diagonal matrix. The aerodynamic characterization of the deck section is usually performed either in the wind, $D - L$, or in the section, $\xi - \eta$, reference system. In particular, assuming aerodynamic coefficients are known in the wind reference system, it is possible to write

$$\boldsymbol{C}_{a,xy} = \boldsymbol{R}\boldsymbol{C}_a, \tag{21}$$

with

$$\boldsymbol{C}_a = \begin{bmatrix} C_D \\ C_L \\ C_M \end{bmatrix}, \qquad \boldsymbol{R} = \begin{bmatrix} \cos(\alpha_{wr}) & -\sin(\alpha_{wr}) & 0 \\ \sin(\alpha_{wr}) & \cos(\alpha_{wr}) & 0 \\ 0 & 0 & 1 \end{bmatrix}, \tag{22}$$

where $\boldsymbol{R}$ is a rotation matrix that allows for the passage from the $D-L$ to the $x-y$ reference systems (its introduction will be particularly useful in the following, as the orientation of the $D-L$ reference system is not fixed with respect to the global $x - y$ reference system).

We noted that both Wagner's and Küssner's functions are well approximated by exponentials (Caracoglia and Jones, 2003), which are the solution of Linear Time-Invariant, LTI, systems. This hints to the possibility of approximating the aerodynamic coefficients as the solution of a LTI (Leishman, 2002; Øiseth et al., 2011; Taha and Rezaei,

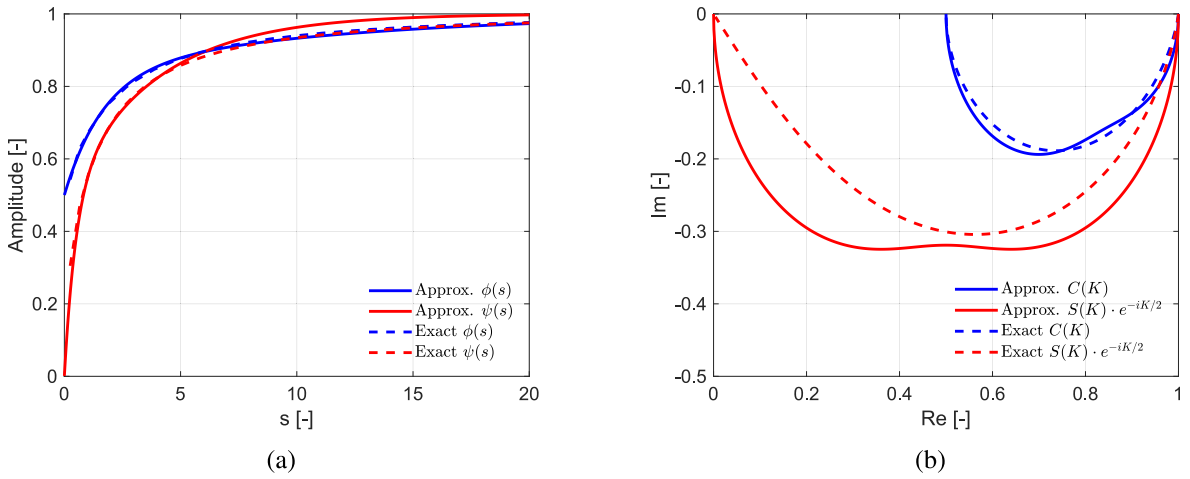


**Fig. 2.** Airfoil theory: comparison between approximate and exact (a) indicial responses and (b) Nyquist plot of the frequency response functions.

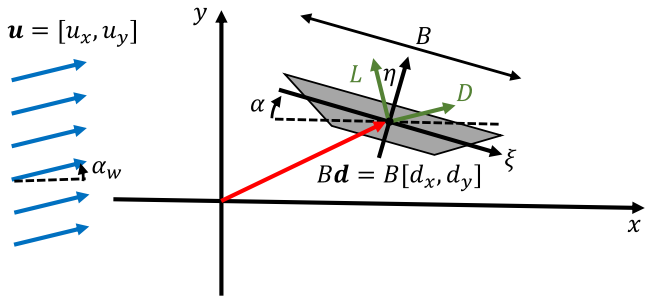


**Fig. 3.** Reference system and sign convention.

2020). We thus postulate aerodynamic coefficients to be expressed, in the surroundings of the equilibrium configuration, by

$$\begin{cases} \dot{\boldsymbol{C}}_r = \boldsymbol{\mathcal{A}}\boldsymbol{C}_r + \boldsymbol{\mathcal{B}}\dot{\boldsymbol{e}} \\ \boldsymbol{C}_a = \boldsymbol{C}_a^{eq}(\alpha_e) + \boldsymbol{\mathcal{C}}\boldsymbol{C}_r + \boldsymbol{\mathcal{D}}\dot{\boldsymbol{e}}, \end{cases} \tag{23}$$

where the calligraphic symbols $\boldsymbol{\mathcal{A}}, \boldsymbol{\mathcal{B}}, \boldsymbol{\mathcal{C}}$ and $\boldsymbol{\mathcal{D}}$ represent matrices collecting model coefficients, and $\boldsymbol{C}_r$ is a vector collecting aerodynamic states. Such states can be interpreted as adjustments to the aerodynamic coefficients to be added to the long-term equilibrium term $\boldsymbol{C}_a^{eq}(\alpha_e)$ in order to account for retarded contributions (which can be either positive or negative). Vector $\boldsymbol{e} = [d_x, d_y, \alpha, \dot{\alpha}]^T$ collects all kinematic parameters that define the velocity of each point of the deck surface (i.e., $\dot{d}_x$, $\dot{d}_y$, $\dot{\alpha}$), as well as $\alpha$, which defines the deck orientation. We assume the velocity scale used to define non-dimensional time to be $U_r$ and that $\mathrm{d}/\mathrm{d}s = B/U_r\ \mathrm{d}/\mathrm{d}t$. We notice that using $U_r$ instead of $U$ is dictated by the necessity to ensure the model consistency in the limit case, for instance, of constant horizontal deck velocity. However, it is here introduced as a reasonable assumption and not as a trivial scaling of time, as it cannot directly be deduced from the rescaling of the problem governing equations. In the case of small oscillations of the deck around an equilibrium configuration, the leading order term of $U_r$ is $U$, recovering the usual non-dimensional time definition. The use of $U_r$ is expected to be accurate in cases for which its value is slowly varying compared to the deck motion, but might be inadequate for other cases.

Denoting as $n_e$, $n_c$ and $n_{cr}$ the lengths of $\boldsymbol{e}$, $\boldsymbol{C}_a$ and $\boldsymbol{C}_r$, respectively, $\boldsymbol{\mathcal{A}}$ is $[n_{cr} \times n_{cr}]$, $\boldsymbol{\mathcal{B}}$ is $[n_{cr} \times n_e]$, $\boldsymbol{\mathcal{C}}$ is $[n_c \times n_{cr}]$ and $\boldsymbol{\mathcal{D}}$ is $[n_c \times n_e]$. We notice that

1. in the presented form, Eqs. (23) are actually not LTI due to the presence of $\boldsymbol{C}_a^{eq}(\alpha_e)$, which can be nonlinear. To obtain a LTI system, it will be sufficient to linearize such term around the value $\bar{\alpha}_e$ of interest;
2. the aerodynamic coefficients automatically tend to the static equilibrium values $\boldsymbol{C}_a^{eq}(\alpha_e)$ quasi-steady response if no excitation occurs and the linear system in the first of Eqs. (23) is stable;
3. Eqs. (23) represent the most general LTI system that links the derivatives of deck kinematic descriptors, $\dot{\boldsymbol{e}}$, to the transient part of aerodynamic coefficients, being the equilibrium part fully and exclusively accounted for by $\boldsymbol{C}_a^{eq}(\alpha_e)$;
4. nonlinearities have been introduced here only in the equilibrium term $\boldsymbol{C}_a^{eq}(\alpha_e)$, which can easily be measured through wind tunnel tests. A more general version of the model, which introduces some nonlinearities also in the aerodynamic states evolution is discussed in Section 3.3.

The problem above is the classical State-Space Model, SSM, representation of a system, linearized in the proximity of a configuration of interest (De Schutter, 2000). In particular, the input vector is represented by the excitations $\dot{\boldsymbol{e}}$, and the output vector are the aerodynamic coefficients. It is noticed that $\boldsymbol{\mathcal{D}}\dot{\boldsymbol{e}}$ is a bypass term, necessary to comply with the airfoil theory, in which it expresses non-circulatory effects.

As it is well known from Control and System Theory, the matrices collecting the model coefficients do not need to be all full. In fact, by rotating the state vector, it is possible to obtain the modal, the controllable and the observable canonical representations of the system (Friedland, 2012). In particular, in modal form $\boldsymbol{\mathcal{B}}, \boldsymbol{\mathcal{C}}$ and $\boldsymbol{\mathcal{D}}$ are full matrices, while $\boldsymbol{\mathcal{A}}$ is at most tri-diagonal (McKelvey and Helmersson, 1996), collecting the system eigenvalues, which can be real or complex conjugate. Assuming, for instance, the system to have eigenvalues $\lambda_1, \lambda_2 \pm i\omega_2, \lambda_3$, the matrix $\boldsymbol{\mathcal{A}}$ in modal form reads

$$\boldsymbol{\mathcal{A}} = \begin{bmatrix} \lambda_1 & 0 & 0 & 0 \\ 0 & \lambda_2 & \omega_2 & 0 \\ 0 & -\omega_2 & \lambda_2 & 0 \\ 0 & 0 & 0 & \lambda_3 \end{bmatrix}. \tag{24}$$

In order to ensure the system stability (see point (2) above), all elements on the diagonal of $\boldsymbol{\mathcal{A}}$ must be strictly negative (further comments are provided in Section 3.4.3). The potential presence of complex eigenvalues enables the oscillatory behavior typical of second-order systems. Summarizing, the model requires as input the time evolution of the deck kinematic descriptors and outputs the time evolution of the aerodynamic forces.

### 3.1. Frequency response function

We now proceed to calculate the FRF between deck motion and aerodynamic forces. For the sake of simplicity and according to usual

wind tunnel practice, we assume here the incoming flow to be horizontal, i.e., $u_x = U$ and $u_y = 0$. With reference to Fig. 3, we introduce the vector $\boldsymbol{w} = [d_x, d_y, \alpha]^T$ and consider small amplitude harmonic deck motions, such that

$$\boldsymbol{w}(K,s) = \tilde{\boldsymbol{w}} e^{iKs}, \quad \boldsymbol{e}(K,s) = \tilde{\boldsymbol{e}} e^{iKs}, \tag{25}$$

where, for the sake of simplicity, the mean value is not considered as the deck is assumed to vibrate in the surroundings of a reference configuration, taken so that $\bar{\boldsymbol{w}} = \boldsymbol{0}$ and $\bar{\boldsymbol{e}} = \boldsymbol{0}$. When the presence of an average angle of attack $\bar{\alpha} \equiv \bar{\alpha}_e$ is relevant, it will explicitly be mentioned. Combining Eqs. (20) and (21), we obtain

$$\boldsymbol{F} = q\boldsymbol{B}\boldsymbol{R}\boldsymbol{C}_a. \tag{26}$$

Assuming, $q$, $\boldsymbol{R}$ and $\boldsymbol{C}_a$ to be linear functions of the input (to be determined by linearization), we obtain

$$\begin{aligned} &\boldsymbol{F}(K,s) = \bar{\boldsymbol{F}} + \tilde{\boldsymbol{F}} e^{iKs}, \; q(K,s) = \bar{q} + \tilde{q} e^{iKs}, \; \boldsymbol{R}(K,s) = (\boldsymbol{I} + \tilde{\boldsymbol{R}} e^{iKs})\bar{\boldsymbol{R}}, \\ &\boldsymbol{C}_a(K,s) = \bar{\boldsymbol{C}}_a + \tilde{\boldsymbol{C}}_a e^{iKs}, \end{aligned} \tag{27}$$

where the different form assumed for the fluctuations related to $\boldsymbol{R}$ is detailed in Appendix A. We also remind that $\boldsymbol{B}$ does not appear as it is a constant matrix. It is then possible to identify the complex amplitude of $\boldsymbol{F}$, $\tilde{\boldsymbol{F}}$, as

$$\tilde{\boldsymbol{F}} = \tilde{q}\boldsymbol{B}\bar{\boldsymbol{R}}\bar{\boldsymbol{C}}_a + \bar{q}\boldsymbol{B}\tilde{\boldsymbol{R}}\bar{\boldsymbol{R}}\bar{\boldsymbol{C}}_a + \bar{q}\boldsymbol{B}\bar{\boldsymbol{R}}\tilde{\boldsymbol{C}}_a, \tag{28}$$

where the first term represents force fluctuations due to variations in the dynamic pressure, the second term accounts for fluctuations in the reference system orientation (here intending the reference system adopted to express aerodynamic coefficients), while the last term accounts for fluctuations in the aerodynamic coefficients induced by deck motion. Further details regarding the determination of $\tilde{\boldsymbol{F}}$ are reported in Appendix A. It is then possible to link $\tilde{q}$, $\tilde{\boldsymbol{R}}$ and $\tilde{\boldsymbol{C}}_a$ to $\tilde{\boldsymbol{w}}$ and rearrange terms in such a way that

$$\tilde{\boldsymbol{F}} = \frac{1}{2}\rho U^2 \boldsymbol{B}[\boldsymbol{H}^q(K) + \boldsymbol{H}^R(K) + \boldsymbol{H}^C(K)]\tilde{\boldsymbol{w}} = \frac{1}{2}\rho U^2 \boldsymbol{B}\boldsymbol{H}(K)\tilde{\boldsymbol{w}}, \tag{29}$$

where the calculation of $\boldsymbol{H}^q(K)$, $\boldsymbol{H}^R(K)$ and $\boldsymbol{H}^C(K)$ is detailed in the following, and $\boldsymbol{H}(K)$ is the sought FRF, which links deck motions to corresponding aerodynamic forces.

### 3.1.1. Calculation of $\boldsymbol{H}^q(K)$

To calculate $\boldsymbol{H}^q(K)$ we firstly need to linearize the dynamic pressure. In particular, remembering that the incoming flow is assumed to be horizontal, we have

$$q = \frac{1}{2}\rho U_r^2 = \frac{1}{2}\rho\left[\left(U - \frac{\mathrm{d}(Bd_x)}{\mathrm{d}t}\right)^2 + \left(\frac{\mathrm{d}(Bd_y)}{\mathrm{d}t}\right)^2\right], \tag{30}$$

which, assuming small deck oscillations, to first-order approximation can be written as

$$q \approx \frac{1}{2}\rho\left(U^2 - 2U\frac{\mathrm{d}(Bd_x)}{\mathrm{d}t}\right) = \frac{1}{2}\rho U^2\left(1 - 2\dot{d}_x\right). \tag{31}$$

Substituting for harmonic oscillations

$$q(K,s) = \bar{q} + \tilde{q}e^{iKs} = \frac{1}{2}\rho U^2(1 - 2iK\tilde{d}_x e^{iKs}), \tag{32}$$

so allowing identifying

$$\tilde{q} = -\rho U^2 iK\tilde{d}_x. \tag{33}$$

As already stated, we notice that, due to the deck motion, the rotation matrix $\boldsymbol{R}$ oscillates. We first rewrite the rotation matrix (see Eq. (22)) linearizing it as

$$\boldsymbol{R} \approx \begin{bmatrix} 1 & -\alpha_{wr} & 0 \\ \alpha_{wr} & 1 & 0 \\ 0 & 0 & 1 \end{bmatrix}. \tag{34}$$

Then, linearizing $\alpha_{wr}$,

$$\alpha_{wr} = \operatorname{atan}\left(\frac{u_{r,y}}{u_{r,x}}\right) \approx \frac{u_{r,y}}{u_{r,x}} = -\frac{\mathrm{d}(Bd_y)}{\mathrm{d}t}\left(U - \frac{\mathrm{d}(Bd_x)}{\mathrm{d}t}\right)^{-1}$$

$$\approx -\frac{B}{U}\frac{\mathrm{d}d_y}{\mathrm{d}t} = -\dot{d}_y, \tag{35}$$

it is then possible to write

$$\boldsymbol{R}(K,s) = \bar{\boldsymbol{R}} + \tilde{\boldsymbol{R}}\bar{\boldsymbol{R}}e^{iKs} = \begin{bmatrix} 1 & iK\tilde{d}_y e^{iKs} & 0 \\ -iK\tilde{d}_y e^{iKs} & 1 & 0 \\ 0 & 0 & 1 \end{bmatrix}, \tag{36}$$

which allows individuating

$$\bar{\boldsymbol{R}} = \begin{bmatrix} 1 & 0 & 0 \\ 0 & 1 & 0 \\ 0 & 0 & 1 \end{bmatrix}, \qquad \tilde{\boldsymbol{R}} = \begin{bmatrix} 0 & iK\tilde{d}_y & 0 \\ -iK\tilde{d}_y & 0 & 0 \\ 0 & 0 & 0 \end{bmatrix}. \tag{37}$$

Looking at Eq. (33) and the first of Eq. (37), we can proceed to write the first term in the right-hand side of Eq. (28) as

$$\tilde{q}\boldsymbol{B}\bar{\boldsymbol{R}}\bar{\boldsymbol{C}}_a = \frac{1}{2}\rho U^2 \begin{bmatrix} -iK2BC_D^{eq}(\bar{\alpha}) & 0 & 0 \\ -iK2BC_L^{eq}(\bar{\alpha}) & 0 & 0 \\ -iK2B^2C_M^{eq}(\bar{\alpha}) & 0 & 0 \end{bmatrix}\tilde{\boldsymbol{w}} = \frac{1}{2}\rho U^2 \boldsymbol{B}\boldsymbol{H}^q(K)\tilde{\boldsymbol{w}}, \tag{38}$$

which defines

$$\boldsymbol{H}^q(K) = \begin{bmatrix} -iK2C_D^{eq}(\bar{\alpha}) & 0 & 0 \\ -iK2C_L^{eq}(\bar{\alpha}) & 0 & 0 \\ -iK2C_M^{eq}(\bar{\alpha}) & 0 & 0 \end{bmatrix}, \tag{39}$$

where the aerodynamic coefficients are calculated at the mean angle of attack.

### 3.1.2. Calculation of $\boldsymbol{H}^R(K)$

We proceed to the calculation of $\boldsymbol{H}^R(K)$ noticing that, looking at the second of Eq. (37), it is possible to rewrite the second term appearing on the right-hand side of Eq. (28) as

$$\bar{q}\boldsymbol{B}\tilde{\boldsymbol{R}}\bar{\boldsymbol{R}}\bar{\boldsymbol{C}}_a = \frac{1}{2}\rho U^2 \begin{bmatrix} B & 0 & 0 \\ 0 & B & 0 \\ 0 & 0 & B^2 \end{bmatrix}\begin{bmatrix} 0 & iK\tilde{d}_y & 0 \\ -iK\tilde{d}_y & 0 & 0 \\ 0 & 0 & 0 \end{bmatrix}\begin{bmatrix} C_D^{eq}(\bar{\alpha}) \\ C_L^{eq}(\bar{\alpha}) \\ C_M^{eq}(\bar{\alpha}) \end{bmatrix}, \tag{40}$$

in which $\bar{\boldsymbol{R}} = \boldsymbol{I}$ has been used. Expressing $\tilde{d}_y$ in terms of $\tilde{\boldsymbol{w}}$, we obtain

$$\bar{q}\boldsymbol{B}\tilde{\boldsymbol{R}}\bar{\boldsymbol{R}}\bar{\boldsymbol{C}}_a = \frac{1}{2}\rho U^2 \begin{bmatrix} 0 & iKBC_L^{eq}(\bar{\alpha}) & 0 \\ 0 & -iKBC_D^{eq}(\bar{\alpha}) & 0 \\ 0 & 0 & 0 \end{bmatrix}\tilde{\boldsymbol{w}} = \frac{1}{2}\rho U^2 \boldsymbol{B}\boldsymbol{H}^R(K)\tilde{\boldsymbol{w}}, \tag{41}$$

where, again, the aerodynamic coefficients are calculated at the mean angle of attack. Then, it follows that:

$$\boldsymbol{H}^R(K) = \begin{bmatrix} 0 & iKC_L^{eq}(\bar{\alpha}) & 0 \\ 0 & -iKC_D^{eq}(\bar{\alpha}) & 0 \\ 0 & 0 & 0 \end{bmatrix}. \tag{42}$$

### 3.1.3. Calculation of $\boldsymbol{H}^C(K)$

We start by linearizing Eqs. (23) and, assuming small amplitude oscillations, we obtain

$$\begin{cases} iK\tilde{\boldsymbol{C}}_r = \boldsymbol{\mathcal{A}}\tilde{\boldsymbol{C}}_r + \boldsymbol{\mathcal{B}}iK\tilde{\boldsymbol{e}}, \\ \tilde{\boldsymbol{C}}_a = \boldsymbol{C}'_a\frac{\mathrm{d}\alpha_e}{\mathrm{d}\boldsymbol{e}}\tilde{\boldsymbol{e}} + \boldsymbol{C}\tilde{\boldsymbol{C}}_r + \boldsymbol{\mathcal{D}}iK\tilde{\boldsymbol{e}}. \end{cases} \tag{43}$$

$\tilde{\boldsymbol{C}}_r$ is the complex amplitude of $\boldsymbol{C}_r$ (see Appendix B for a more complete demonstration considering the dependence of model matrices on the input) and

$$\boldsymbol{C}'_a = \begin{bmatrix} C'_D \\ C'_L \\ C'_M \end{bmatrix}, \qquad \frac{\mathrm{d}\alpha_e}{\mathrm{d}\boldsymbol{e}} = \begin{bmatrix} 0 & -1 & 1 & 0 \end{bmatrix}, \tag{44}$$

where the derivatives of the aerodynamic coefficients shall be evaluated in the proximity of the mean angle of attack $\bar{\alpha}$. From the first of

Eqs. (43), we obtain

$$\tilde{\boldsymbol{C}}_r = \left[iK\boldsymbol{I} - \boldsymbol{\mathcal{A}}\right]^{-1} iK\boldsymbol{\mathcal{B}}\tilde{\boldsymbol{e}}, \tag{45}$$

where $\boldsymbol{I}$ is the identity matrix. Substituting it in the second of Eqs. (43), yields

$$\tilde{\boldsymbol{C}}_a = \left\{ \boldsymbol{C}'_a \frac{\mathrm{d}\alpha_e}{\mathrm{d}\boldsymbol{e}} + \boldsymbol{C}\left[iK\boldsymbol{I} - \boldsymbol{\mathcal{A}}\right]^{-1} iK\boldsymbol{\mathcal{B}} + iK\boldsymbol{\mathcal{D}} \right\} \tilde{\boldsymbol{e}}. \tag{46}$$

We now notice that

$$\tilde{\boldsymbol{e}} = \begin{bmatrix} \tilde{d}_x \\ \tilde{d}_y \\ \tilde{\alpha} \\ \tilde{\dot{\alpha}} \end{bmatrix} = \begin{bmatrix} iK & 0 & 0 \\ 0 & iK & 0 \\ 0 & 0 & 1 \\ 0 & 0 & iK \end{bmatrix} \begin{bmatrix} \tilde{d}_x \\ \tilde{d}_y \\ \tilde{\alpha} \end{bmatrix} = \boldsymbol{T}\tilde{\boldsymbol{w}}, \tag{47}$$

so defining matrix $\boldsymbol{T}$. Looking at Eq. (46) and remembering that $\bar{\boldsymbol{R}}$ is the identity matrix, it is then possible to write the last term of the right-hand side of Eq. (28) as

$$\begin{aligned} \bar{q}\boldsymbol{B}\bar{\boldsymbol{R}}\tilde{\boldsymbol{C}}_a &= \frac{1}{2}\rho U^2 \boldsymbol{B}\left\{ \boldsymbol{C}'_a \frac{\mathrm{d}\alpha_e}{\mathrm{d}\boldsymbol{e}} + \boldsymbol{C}\left[iK\boldsymbol{I} - \boldsymbol{\mathcal{A}}\right]^{-1} iK\boldsymbol{\mathcal{B}} + iK\boldsymbol{\mathcal{D}} \right\} \boldsymbol{T}(K)\tilde{\boldsymbol{w}} \\ &= \frac{1}{2}\rho U^2 \boldsymbol{B}\boldsymbol{H}^C(K)\tilde{\boldsymbol{w}} \end{aligned} \tag{48}$$

which defines

$$\boldsymbol{H}^C(K) = \left\{ \boldsymbol{C}'_a \frac{\mathrm{d}\alpha_e}{\mathrm{d}\boldsymbol{e}} + \boldsymbol{C}\left[iK\boldsymbol{I} - \boldsymbol{\mathcal{A}}\right]^{-1} iK\boldsymbol{\mathcal{B}} + iK\boldsymbol{\mathcal{D}} \right\} \boldsymbol{T}(K). \tag{49}$$

In Eq. (49), quasi-static contributions are completely represented by the first term only.

Once $\boldsymbol{H}^q(K)$, $\boldsymbol{H}^R(K)$ and $\boldsymbol{H}^C(K)$ are determined, summing them as prescribed by Eq. (29), it is possible to obtain $\boldsymbol{H}(K)$.

#### 3.1.4. Quasi-static response

It is of interest to specialize the obtained FRF to the quasi-static case. To this purpose, looking at Eq. (49), we set $\boldsymbol{C} = \boldsymbol{\mathcal{D}} = \boldsymbol{0}$, so eliminating the contribution of aerodynamic states and bypass terms. Under such assumption, the quasi-static FRF, $\boldsymbol{H}^{qs}$, is obtained in agreement with Eq. (29) as

$$\boldsymbol{H}^{qs} = \begin{bmatrix} -iK2C_D^{eq}(\bar{\alpha}) & iK[C_L^{eq}(\bar{\alpha}) - C'_D] & C'_D \\ -iK2C_L^{eq}(\bar{\alpha}) & -iK[C_D^{eq}(\bar{\alpha}) + C'_L] & C'_L \\ -iK2C_M^{eq}(\bar{\alpha}) & -iKC'_M & C'_M \end{bmatrix}, \tag{50}$$

which coincides with the well-known result reported for instance by Diana et al. (1993).

#### 3.1.5. Identification of flutter derivatives

Flutter derivatives can be extracted from $\boldsymbol{H}(K)$ identifying its components as

$$\boldsymbol{H}(K) = \begin{bmatrix} P_6^* + iP_5^* & P_4^* + iP_1^* & P_3^* + iP_2^* \\ H_6^* + iH_5^* & H_4^* + iH_1^* & H_3^* + iH_2^* \\ A_6^* + iA_5^* & A_4^* + iA_1^* & A_3^* + iA_2^* \end{bmatrix} K^2. \tag{51}$$

Different conventions are used in the literature for naming the flutter derivatives. In the present contribution, the use of the symbols is self-evident considering the ordering of $\boldsymbol{F}$ and $\boldsymbol{w}$ vectors. It is finally possible to express, according to the commonly adopted mixed time-frequency formulation (see Eq. (12)), aerodynamic forces and moments due to sinusoidal deck motions as

$$\begin{aligned} F_x(K,s) = \frac{1}{2}\rho U^2 B \Big[ & C_x^{eq}(\bar{\alpha}) + K^2 P_6^* d_x + KP_5^* \dot{d}_x + K^2 P_4^* d_y + KP_1^* \dot{d}_y \\ & + K^2 P_3^* \alpha + KP_2^* \dot{\alpha} \Big], \end{aligned} \tag{52}$$

$$\begin{aligned} F_y(K,s) = \frac{1}{2}\rho U^2 B \Big[ & C_y^{eq}(\bar{\alpha}) + K^2 H_6^* d_x + KH_5^* \dot{d}_x + K^2 H_4^* d_y + KH_1^* \dot{d}_y \\ & + K^2 H_3^* \alpha + KH_2^* \dot{\alpha} \Big], \end{aligned} \tag{53}$$

$$\begin{aligned} M(K,s) = \frac{1}{2}\rho U^2 B^2 \Big[ & C_m^{eq}(\bar{\alpha}) + K^2 A_6^* d_x + KA_5^* \dot{d}_x + K^2 A_4^* d_y + KA_1^* \dot{d}_y \\ & + K^2 A_3^* \alpha + KA_2^* \dot{\alpha} \Big]. \end{aligned} \tag{54}$$

We can stress here that: (i) contrarily to the usual notation (Scanlan, 1993), non-dimensional displacements $d_x$ and $d_y$ have been used, and derivatives are taken with respect to non-dimensional time; (ii) the mixed time-frequency formulation shall not be misinterpreted, as it is actually deduced in the frequency domain and, as such, is valid only for sinusoidal deck motions; (iii) in most applications, the effects of $d_x$ and $P^*$-flutter derivatives are not determinant for flutter stability; in contrast, they play an important role in lateral buffeting response, which is known to be crucial for stress checks in the deck (e.g., Barni et al. (2023)). It is also worth noting that the inherent inconsistency of mixed time-frequency formulation leads to several shortcomings, preventing the use of integral transformations and requiring iterative procedures for the stability assessment of linear systems. Finally, the interested Reader is invited to refer to Appendix C for the derivation of the FRF considering a representation of the aerodynamic coefficients based on the $\xi - \eta$ reference system.

### 3.2. Airfoil

The presented model can easily be particularized to provide the results presented in Section 2 for the airfoil theory, in the approximate version summarized in Eqs. (5) and (10). In particular, we can rewrite the downwash angle reported in Eq. (2) as

$$\alpha_{dw}(s) = \alpha(s) + \beta\dot{\alpha}(s) - \dot{d}_y(s), \tag{55}$$

where the parameter $\beta = 1/4$ has been introduced for the sake of clarity. Jones's approximation (see Eq. (5)) thus reads

$$\phi(s) = 1 - de^{-\delta s} - ge^{-\gamma s}. \tag{56}$$

The SSM for the airfoil is then characterized by

$$\begin{aligned} &\boldsymbol{e} = \begin{bmatrix} \dot{d}_y \\ \alpha \\ \dot{\alpha} \end{bmatrix}, \quad \boldsymbol{\mathcal{A}} = -\begin{bmatrix} \delta & 0 \\ 0 & \gamma \end{bmatrix}, \quad \boldsymbol{\mathcal{B}} = C'_L \begin{bmatrix} d & d\beta & -d \\ g & g\beta & -g \end{bmatrix}, \\ &\boldsymbol{C} = -\begin{bmatrix} 1 & 1 \\ 1/4 & 1/4 \end{bmatrix}, \end{aligned} \tag{57}$$

where $C'_L = 2\pi$, and the terms $1/4$ appearing in $\boldsymbol{C}$ account for the fact that the lift is applied at the quarter chord point. In addition, the rows of $\boldsymbol{\mathcal{B}}$ and $\boldsymbol{C}$ are linearly dependent due to the airfoil special simplicity.

As regard the bypass term $\boldsymbol{\mathcal{D}}$, it is useful to divide it into two parts. The first part, $\boldsymbol{\mathcal{D}}^{nc}$, accounts for non-circulatory terms, while the second part, $\boldsymbol{\mathcal{D}}^{c}$, compensates for the fact that the contribution $\beta\dot{\alpha}$ has been neglected in the calculation of the quasi-static terms (see Eq. (19)). It is thus a feature of the present model to disregard $\dot{\alpha}$ in the quasi-static contributions, noticing that it can be in fact incorporated in other terms. Actually, the inclusion of $\dot{\alpha}$ in $\alpha_e$ would introduce a redundant unknown parameter in Eq. (19) (i.e., the parameter $\beta$ in Eq. (55)). Summarizing, we can write

$$\boldsymbol{\mathcal{D}} = \boldsymbol{\mathcal{D}}^{nc} + \boldsymbol{\mathcal{D}}^{c}, \tag{58}$$

with

$$\boldsymbol{\mathcal{D}}^{nc} = \begin{bmatrix} \pi/2 & 0 & -\pi/2 \\ -\pi/8 & -\pi/64 & 0 \end{bmatrix}, \qquad \boldsymbol{\mathcal{D}}^{c} = C'_L\beta \begin{bmatrix} 1 & 0 & 0 \\ 1/4 & 0 & 0 \end{bmatrix}. \tag{59}$$

Concerning the FRF, for the airfoil at zero incidence angle, $C_L^{eq}(\bar{\alpha}) = C_M^{eq}(\bar{\alpha}) = 0$, so that the only contributions to $\boldsymbol{H}(K)$ are due to $\boldsymbol{H}^C(K)$ (i.e., $\boldsymbol{H}^q(K) = \boldsymbol{0}$ and $\boldsymbol{H}^R(K) = \boldsymbol{0}$).

We finally notice that the described SSM does contain some redundant parameters. For instance, the system characterized by $\varepsilon\boldsymbol{\mathcal{B}}$ and $\boldsymbol{C}/\varepsilon$ is equivalent to that with $\boldsymbol{\mathcal{B}}$ and $\boldsymbol{C}$, with $\varepsilon$ arbitrary constant. The number of redundant parameters is the minimum between model inputs and outputs, and such aspect shall be tackled during the system calibration by introducing regularization terms in the fitting target function, as described in Section 3.4.

### 3.3. Relation to other models and generalizations

Before proceeding, we notice that the SSM described in Eq. (23) takes as input the derivative of vector $\boldsymbol{e}$, $\dot{\boldsymbol{e}} = [\ddot{d}_x, \ddot{d}_y, \dot{\alpha}, \ddot{\alpha}]^T$, which collects second-order derivatives of all deck kinematic degrees of freedom, as well as $\dot{\alpha}$. However, the model can be recasted in such a way that the forcing term of the aerodynamic states is represented by $\boldsymbol{e}$ (see Appendix D). Then, it can be concluded that:

1. for the present model, the order of the derivatives appearing in the forcing term of the aerodynamic states is not substantial;
2. considering both $\alpha$ and $\dot{\alpha}$ in $\boldsymbol{e}$ is redundant. This redundancy has been retained to allow for better individuation of each contribution, more closely resembling the structure of thin-airfoil theory.

The price to pay for recasting the model taking $\boldsymbol{e}$ as forcing term of the aerodynamic states is that quasi-static contributions are no longer clearly separate from the others. Keeping such terms distinct is indeed desirable, as it allows imposing *a priori* the consistency with measured long-term equilibrium aerodynamic forces, rather than obtaining it *a posteriori*, based on the fitting of flutter derivatives at high reduced velocities.

#### 3.3.1. Rational function approximation

We start by considering the Rational Function Approximation, RFA, as described for instance in Roger (1977), Chen and Kareem (2001) and Barni et al. (2021). In such an approach, we approximate the FRF, $\boldsymbol{H}(K)$, (usually known through flutter derivatives) as

$$\boldsymbol{H}(K) \approx \boldsymbol{\mathcal{M}}_1 + iK\boldsymbol{\mathcal{M}}_2 + (iK)^2\boldsymbol{\mathcal{M}}_3 + \sum_{n=1}^{N} \boldsymbol{\mathcal{M}}_{n+3} \frac{iK}{iK + d_n}. \tag{60}$$

where $\boldsymbol{\mathcal{M}}_i$ are matrices collecting coefficients to be calibrated, $N$ shall be chosen to approximate $\boldsymbol{H}(K)$ to an acceptable accuracy, and $d_n$ are positive real values. The approximate transfer function has the following time-domain equivalent:

$$\boldsymbol{C}_a(s) = \boldsymbol{\mathcal{M}}_1\boldsymbol{w}(s) + \boldsymbol{\mathcal{M}}_2\dot{\boldsymbol{w}}(s) + \boldsymbol{\mathcal{M}}_3\ddot{\boldsymbol{w}}(s) + \sum_{n=1}^{N} \boldsymbol{\mathcal{M}}_{l+3}\boldsymbol{\phi}_n(s), \tag{61}$$

where $\boldsymbol{\phi}_n(s)$ are vectors collecting triplets of aerodynamic states (one triplet of aerodynamic states for each element of $\boldsymbol{w}$). Such triplets evolve in time as

$$\dot{\boldsymbol{\phi}}_n = -d_n\boldsymbol{\phi}_n + \dot{\boldsymbol{w}}. \tag{62}$$

Comparing Eqs. (61) and (62) to Eq. (23), it is possible to see that the models are formally similar, being the aerodynamic states collected in the triplets $\boldsymbol{\phi}_n$ analogous to $\boldsymbol{C}_r$. The excitation of the aerodynamic states for the RFA model is represented by $\dot{\boldsymbol{w}}$ (collecting first-order derivatives of the deck kinematic degrees of freedom), while for the present model is $\dot{\boldsymbol{e}}$ (which collects second-order derivatives plus the first-order derivative of the rotation). Such difference is not substantial (see Appendix D) and leads, for the standard RFA model, to a mixing of quasi-static and purely unsteady contributions. In fact, an RFA formulation that solves the problem has been proposed in Øiseth et al. (2011), by introducing $\ddot{\boldsymbol{w}}$ as forcing term.

It can thus be concluded that the present model is a generalization of the RFA approach. In particular, despite the specific RFA formulation, we notice that:

1. in the RFA model, $d_n$ are real positive values, so restricting the nature of the system eigenvalues collected in $\boldsymbol{\mathcal{A}}$ (i.e., according to Eq. (24)). This precludes the model to represent complex eigenvalues typical, for instance, of first-order systems derived from second-order ones;

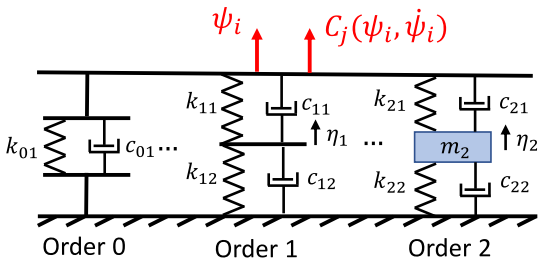


**Fig. 4.** Schematization of rheological models.

2. in the RFA model, triplets of aerodynamic states characterized by the same eigenvalue $-d_n$ evolve according to Eq. (62). Substantially, exploiting the system linearity, each triplet represents the state evolution assuming only one component of $\boldsymbol{w}$ is present at a time. Then, their contribution is weighted according to $\boldsymbol{\mathcal{M}}_{n+3}$, superimposing all effects. This approach produces an unnecessary proliferation of aerodynamic states, which might burden numerical integration in time-domain analyses.

#### 3.3.2. Rheological models

As regards Rheological Models, RMs, we consider the schematization reported in Calamelli et al. (2024) and Diana et al. (2013), see Fig. 4. They consist in a series of oscillators, operating in parallel, of order 0, 1 and 2, ideally connected on one side to a restraint and, on the other side, to a common degree of freedom $\psi_i$, which represents a deck kinematic degree of freedom. As reported in Diana et al. (2013), each aerodynamic force component is modeled with a specific rheological model.

Considering the equilibrium of the transversal bar to which all oscillators are connect, for the simple case of Fig. 4, one obtains:

$$C_j(\psi, \dot{\psi}) - F_0 - F_1 - F_2 = 0, \tag{63}$$

being $F_0$, $F_1$ and $F_2$ the forces transmitted by the oscillators of order 0, 1 and 2, respectively. It is thus possible to write:

$$C_j(\psi, \dot{\psi}) = k_{01}\psi + c_{01}\dot{\psi} + k_{11}(\psi - \eta_1) + c_{11}(\dot{\psi} - \dot{\eta}_1) + k_{21}(\psi - \eta_2) + c_{21}(\dot{\psi} - \dot{\eta}_2), \tag{64}$$

which, denoting $\boldsymbol{\psi} = [\psi, \dot{\psi}]^T$ and $\boldsymbol{\eta} = [\eta_1, \dot{\eta}_1, \eta_2, \dot{\eta}_2]^T$, can be rearranged as

$$C_j(\psi, \dot{\psi}) = \boldsymbol{\mathcal{C}}\boldsymbol{\eta} + \boldsymbol{\mathcal{D}}\boldsymbol{\psi}. \tag{65}$$

The equation is formally similar to the second of Eq. (23) but, in this case, the time derivative of the aerodynamic states contribute to the aerodynamic forces. However, this can also be obtained in the proposed model as, from the first of Eq. (23), $\dot{\boldsymbol{C}}_r$ is a linear combination of $\boldsymbol{C}_r$ and $\dot{\boldsymbol{e}}$, which can be rearranged and substituted in the second of Eq. (23).

As regard the first of Eq. (23), its analogous for RMs is deduced by the dynamic equilibrium of the oscillators. Still looking at Fig. 4, for oscillators of order 1, the equilibrium of the degree of freedom $\eta_1$ requires:

$$k_{11}(\eta_1 - \psi) + k_{12}\eta_1 + c_{11}(\dot{\eta}_1 - \dot{\psi}) + c_{12}\dot{\eta}_1 = 0, \tag{66}$$

which can be rearranged as

$$(k_{11} + k_{12})\eta_1 + (c_{11} + c_{12})\dot{\eta}_1 = k_{11}\psi + c_{11}\dot{\psi}, \tag{67}$$

so leading to

$$\dot{\eta}_1 = -\frac{k_{11} + k_{12}}{c_{11} + c_{12}}\eta_1 + \frac{k_{11}}{c_{11} + c_{12}}\psi + \frac{c_{11}}{c_{11} + c_{12}}\dot{\psi}, \tag{68}$$

which can be rewritten as

$$\dot{\eta}_1 = \mathcal{A}\eta_1 + \boldsymbol{\mathcal{B}}\boldsymbol{\psi}. \tag{69}$$

The equation is similar to that ruling the aerodynamic states in the present model, being the main difference that the deck kinematic degrees of freedom and their first-order derivatives appear instead of the second-order derivatives used in the present model (complemented by the first-order derivative of the rotation). However, this point is not substantial, as already discussed above and shown in Appendix D.

Similar considerations can be made for oscillators of order 2, which allow introducing complex eigenvalues and, thus, an oscillatory behavior of the aerodynamic states, as in the proposed model.

Overall, RMs closely resemble the proposed model with two main differences:

1. in RMs, the nature of the eigenvalues (real or complex) is fixed *a priori*, while in the proposed model the system is able to adapt automatically;
2. in RMs, different aerodynamic coefficients cannot share the same aerodynamic states, generally leading to the necessity of duplicating them.

Therefore, available models, despite assuming different forms, share the same intrinsic structure and essentially differ in:

1. the possibility of accounting for the presence of complex eigenvalues for the aerodynamic states;
2. the possibility of sharing aerodynamic states between different aerodynamic coefficients and deck kinematic degrees of freedom;
3. the number of redundant model coefficients;
4. the order of the derivatives of deck kinematic degrees of freedom that excite the aerodynamic states. This feature, however, does not affect the model generality, rather being an obstacle to a clear splitting of quasi-static contributions from other terms, if not properly formulated.

As previously discussed, the present model appears to be an optimal choice with respect to all features above, providing a good balance between model simplicity and clarity (i.e., through a careful splitting of quasi-static and purely transient terms), generality (i.e., allowing for an automatic choice between real and complex eigenvalues) and computational efficiency (i.e., allowing for the sharing of aerodynamic states between different aerodynamic coefficients and deck kinematic degrees of freedom).

#### 3.3.3. Generalizations

As the present model represents a reorganization and generalization of RFA and rheological models, techniques used in such contexts can directly be applied here as well. In particular, we briefly remind that the advantage of time-domain formulations for motion-induced forces mainly lies in the possibility of introducing nonlinearities in bridge buffeting and random flutter analyses (e.g., Chen and Kareem (2001), Pospíšil et al. (2006), Barni and Mannini (2024) and Barni et al. (2024)). In general, the incoming fluctuating velocity components could be added to the vector $\boldsymbol{e}$ and, thus, $\boldsymbol{w}$, leading to $\boldsymbol{e} = [\dot{d}_x, \dot{d}_y, \alpha, \dot{\alpha}, u_x/U, u_y/U]^T$. The model would then provide as output both motion-induced and buffeting forces and shall properly be expanded and calibrated including also information regarding the deck aerodynamic admittance.

The nonlinear term $\boldsymbol{C}_a^{eq}(\alpha_e)$ in Eq. (23) naturally allows considering nonlinearities in the aerodynamic coefficients. However, it has been found in the use of similar models (i.e., RFA and RMs) that, in order to obtain accurate results, it is necessary to consider a dependency of $\boldsymbol{\mathcal{A}}$, $\boldsymbol{\mathcal{B}}$, $\boldsymbol{C}$ and $\boldsymbol{\mathcal{D}}$ on the slowly-varying angle of attack to account for the dependence of flutter derivatives on the mean angle of attack. Therefore, the incoming wind velocity field is usually split into low- and high-frequency components (band-superposition approach). In particular, by using a low-pass filter, it is possible to write:

$$\boldsymbol{u} = \boldsymbol{u}^{LF} + \boldsymbol{u}^{HF}, \tag{70}$$

where $LF$ and $HF$ indicate the low- and high- frequency components, respectively. We denote as $\alpha^{LF}$ the slowly-varying angle of attack of the incoming wind $\alpha^{LF} = \mathrm{atan}(u_y^{LF}/u_x^{LF})$. In the simplest form, in which we assume the angle of attack due to the incoming gusts dominant compared to that due to the deck motion (Barni et al., 2022), Eq. (23) can be written as:

$$\begin{cases} \dot{\boldsymbol{C}}_r = \boldsymbol{\mathcal{A}}(\alpha^{LF})\boldsymbol{C}_r + \boldsymbol{\mathcal{B}}(\alpha^{LF})\dot{\boldsymbol{e}} \\ \boldsymbol{C}_a = \boldsymbol{C}_a^{eq}(\alpha^{LF}) + \boldsymbol{C}_a'(\alpha^{LF})\frac{\mathrm{d}\alpha_e}{\mathrm{d}\boldsymbol{e}}\boldsymbol{e} + \boldsymbol{C}(\alpha^{LF})\boldsymbol{C}_r + \boldsymbol{\mathcal{D}}(\alpha^{LF})\dot{\boldsymbol{e}}, \end{cases} \tag{71}$$

where the matrices $\boldsymbol{\mathcal{A}}(\alpha^{LF})$, $\boldsymbol{\mathcal{B}}(\alpha^{LF})$, $\boldsymbol{C}(\alpha^{LF})$ and $\boldsymbol{\mathcal{D}}(\alpha^{LF})$ shall be calibrated feeding the flutter derivatives and aerodynamic admittance functions at different angles of attack, while excitations now are $\boldsymbol{e} = [\dot{d}_x, \dot{d}_y, \alpha, \dot{\alpha}, u_x^{HF}/u_x^{LF}, u_y^{HF}/u_x^{LF}]^T$.

The extension presented in Eq. (71) is only one of the possible approaches and, in particular, the treatment of the term $\boldsymbol{C}_a^{eq}(\alpha^{LF})$ might be improved with known techniques, such as the Corrected Quasi-Steady Theory (Diana et al., 2013). The choice of the cut-off frequency is known to be crucial (Wu and Kareem, 2013), and the multiple cut-off strategy has been devised in Barni et al. (2022) to minimize its impact. Research is still needed on this topic and, while the approach based on low/high frequency velocity components splitting has proved effective and accurate in many circumstances (Barni et al., 2022; Barni and Mannini, 2024), it makes the approach deviate from a pure time-domain formulation, which is in principle the best suited one to treat system nonlinearities.

### 3.4. Model implementation and calibration

The model implementation does not need particular precaution for the construction of matrices $\boldsymbol{\mathcal{B}}$, $\boldsymbol{C}$ and $\boldsymbol{\mathcal{D}}$. The coefficients there appearing are parameters to be optimized in order to minimize an error function which is further detailed in Section 3.4.3. If the model is adopted in the form presented in Eqs. (71) (with the model matrices depending on $\alpha^{LF}$), each term in the matrices can be approximated by means of a polynomial expansion in $\alpha^{LF}$, whose coefficients are the optimization variables (Barni et al., 2021). However, as discussed above, the present model requires the eigenvalues collected in the matrix $\boldsymbol{\mathcal{A}}$ to have all negative real part to ensure system stability, i.e., guarantee that aerodynamic forces tend to those expected at equilibrium. To this purpose, we can distinguish two possible operating modes for the model, which are detailed below.

#### 3.4.1. Diagonal mode

In the diagonal mode, the model becomes equivalent to the RFA approach. In particular, we postulate all eigenvalues to be real, so that all coefficients appearing on the diagonal of $\boldsymbol{\mathcal{A}}$ are real and negative, while, according to Eq. (24), no term shall appear outside the diagonal. We then define a vector of parameters $\boldsymbol{A}$ (of length equal to the number of considered aerodynamic states, $n_{cr}$), such that the terms on the diagonal of $\boldsymbol{\mathcal{A}}$ are $\mathcal{A}_{j,j} = -A_j^2$. In this way, the stability of the system is imposed *a priori*. If the model is nonlinear, we will have $\boldsymbol{\mathcal{A}}(\alpha^{LF})$, and the components of the vector $\boldsymbol{A}$ are approximated with a polynomial expansion, so as to always preserve the system stability.

#### 3.4.2. General mode

In the general mode, the model allows for the presence of both real and complex eigenvalues. The number of real values needed to characterize $\boldsymbol{\mathcal{A}}$ is identical to that required when operating in *diagonal mode* (i.e., the number of aerodynamic states). Indeed, taking a pair of eigenvalues, they can only be either real and distinct or complex conjugates, in both cases requiring only two parameters (real numbers) for their representation. We build the vector $\boldsymbol{A}$ as for the *diagonal mode*. Then, for the indices $j$ and $j+1$ we calculate

$$r_{j1} = A_j + \sqrt{A_{j+1}}, \qquad r_{j2} = A_j - \sqrt{A_{j+1}}, \tag{72}$$

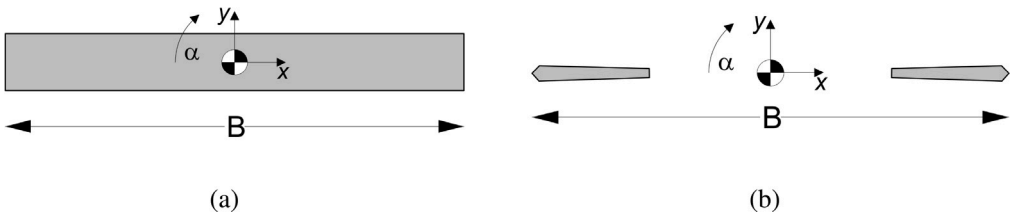


**Fig. 5.** Geometry of the sections analyzed for the linear model: (a) R8 and (b) Gibraltar Bridge deck.

then we impose

$$\mathcal{A}_{j,j} = -\mathrm{Re}(r_{j1})^2, \quad \mathcal{A}_{j+1,j+1} = -\mathrm{Re}(r_{j2})^2, \quad \mathcal{A}_{j,j+1} = -\mathcal{A}_{j+1,j} = \mathrm{Im}(r_{j1}). \tag{73}$$

where the functions Re and Im extract the real and imaginary part of the input, respectively. The vector $\boldsymbol{A}$ thus represents a parametrization of $\boldsymbol{\mathcal{A}}$, which enforces *a priori* the system stability. Also in this case, if $\boldsymbol{\mathcal{A}}$ depends on $\alpha^{LF}$, it is possible to proceed with a polynomial expansion of the components of $\boldsymbol{A}$.

### 3.4.3. Error function

We report here some considerations regarding the error function definition, valid irrespectively of the fact that the model is operated in *diagonal* or *general* mode, and of the possible dependency of model matrices on $\alpha^{LF}$. We assume flutter derivatives to be known, so that $\boldsymbol{H}(K)$ can be evaluated using Eq. (51). We denote the measured $\boldsymbol{H}(K)$ as $\boldsymbol{H}^m(K_j)$ and assume that its components are known at the reduced frequencies $K_j$, $j = 1, 2...J$. Firstly, we build two scaling matrices such that:

$$\begin{aligned} \boldsymbol{S}_{Re} &= \left\{ \frac{1}{J} \sum_{j=1}^{J} |\mathrm{Re}(\boldsymbol{H}^m(K_j) K_j^2)| \right\}^{\textcircled{-1}}, \\ \boldsymbol{S}_{Im} &= \left\{ \frac{1}{J} \sum_{j=1}^{J} |\mathrm{Im}(\boldsymbol{H}^m(K_j) K_j^2)| \right\}^{\textcircled{-1}}, \end{aligned} \tag{74}$$

where element-wise operations are denoted as circled, and $||$ is the absolute value. Such scaling matrices are used to make the weight of all flutter derivatives comparable within the fitting. We collect all parameters necessary to build the model matrices $\boldsymbol{\mathcal{A}}$, $\boldsymbol{\mathcal{B}}$, $\boldsymbol{C}$ and $\boldsymbol{D}$ in the vector $\boldsymbol{P}$. Finally, we write:

$$err_{H,Re} = \sum_{j=1}^{J} \left\{ \left| \mathrm{Re}\left( \frac{\boldsymbol{H}^m(K_j) - \boldsymbol{H}(K_j)}{K_j^2} \right) \odot \boldsymbol{S}_{Re} \right|^2 \left[ (1-\mu_K) + \mu_K \frac{K_j^4}{K_{max}^4} \right] \right\}, \tag{75}$$

where $|\,|^2$ indicates the squared $L-2$ norm, $\odot$ is the element-wise product, $K_{max}$ is the maximum sampled reduced frequency, and $\mu_K$ is a parameter that regulates the relative weights to be given to the error calculated on $\boldsymbol{H}(K)/K^2$ (i.e., flutter derivatives) and $\boldsymbol{H}(K)$ (i.e., the RFR). In particular, the first error contribution privileges small reduced frequencies (i.e., high reduced velocities), while the second contribution gives more importance to high reduced frequencies (i.e., small reduced velocities). Analogously, we calculate:

$$err_{H,Im} = \sum_{j=1}^{J} \left\{ \left| \mathrm{Im}\left( \frac{\boldsymbol{H}^m(K_j) - \boldsymbol{H}(K_j)}{K_j^2} \right) \odot \boldsymbol{S}_{Im} \right|^2 \left[ (1-\mu_K) + \mu_K \frac{K_j^4}{K_{max}^4} \right] \right\}. \tag{76}$$

The error function used in the optimization is then defined as:

$$err = \left( err_{H,Re} + err_{H,Im} \right)^{\frac{1}{2}} \left[ 1 + \mu_P \frac{|\boldsymbol{P}|}{n_P} + \sum_{l=1}^{n_{cr}} \frac{\mu_D}{|\mathcal{A}_{ll}|} \right], \tag{77}$$

where $n_P$ is the total number of model coefficients (the components of $\boldsymbol{P}$), while $\mu_P$ and $\mu_D$ are constants to be fixed *a priori*. The error $err_H = err_{H,Re} + err_{H,Im}$ is amplified by two factors. The first one is a regularization term, which penalizes high modules for the components of $\boldsymbol{P}$ (the technique is classical, aiming at contrasting overfitting, see for instance Müller and Guido, 2016). This also allows solving the indeterminacy due to the presence of redundant parameters, as described in Section 3.2, allowing individuating a well-defined unique solution to the minimization. The second term penalizes the occurrence of very small values on the diagonal of $\boldsymbol{\mathcal{A}}$. Indeed, though following the procedure presented in Sections 3.4.1 and 3.4.2 allows imposing negative real part for all eigenvalues, it is still possible for them to approach a null value. In such conditions, the delay terms would tend to decay in a very long time (or not to decay at all in the limit of a null value), introducing modifications to the long-term system response (i.e., effectively modifying the quasi-static terms), which is not the intended behavior. Both penalizations are introduced as multipliers of the error, in such a way that the points in the parameters space for which $err_H = 0$ are unaffected.

In the following, after numerical experimentation, we always select $\mu_K = 0.1$, $\mu_P = 0.1$ and $\mu_D = 0.001$, and adopt the Broyden–Fletcher–Goldfarb–Shanno algorithm for the minimization of the error function. The minimization is performed several times starting at random points and the one characterized by the smallest final error is retained (5 starting points are used in the following).

## 4. Results

In this section, we present some results obtained applying the proposed model. In particular, we start by fitting the model to the airfoil, for which the analytical solution is available, and to two sections characterized by very different aerodynamic properties. In these cases, the model coefficients are all constants and, so, we denote the model as linear (see Eq. (23)). Then, we consider two bridge deck sections for which flutter derivatives are known at different angles of attack. In this case, a polynomial expansion of the model coefficients is adopted and, so, we denote the model as nonlinear (see Eq. (71)).

### 4.1. Linear model

As anticipated, we now proceed to the model calibration assuming constant coefficients. We consider a thin-airfoil and two sections: a rectangle with aspect ratio 1:8, denoted as R8, and a simplified model of the Gibraltar Bridge deck. The measured flutter derivatives are both taken from Starossek et al. (2009), which the Reader can consult for details regarding the experimental results. Briefly, flutter derivatives were extracted using forced vibrations in a water channel, obtaining a good characterization of the aerodynamic behavior also in the small reduced velocity range (up to $U_{red} = 2\pi/K \approx 1$). The geometry of the two considered sections is reported in Fig. 5, while Fig. 6 shows the corresponding equilibrium (i.e., static) aerodynamic coefficients.

The SSM performance is analyzed considering a varying number of internal states when the *general* formulation is adopted. A comparison between the target flutter derivatives and those obtained after calibration of the SSM model considering two and six aerodynamic

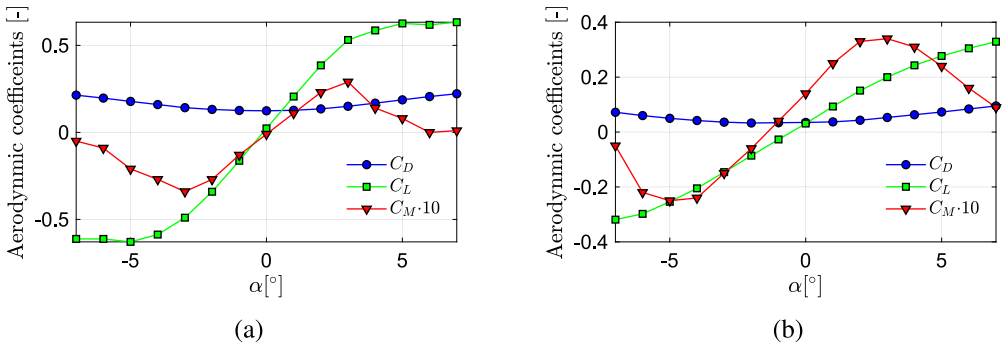


**Fig. 6.** Equilibrium aerodynamic coefficients of the sections analyzed for the linear model: (a) R8 (b) Gibraltar Bridge deck.

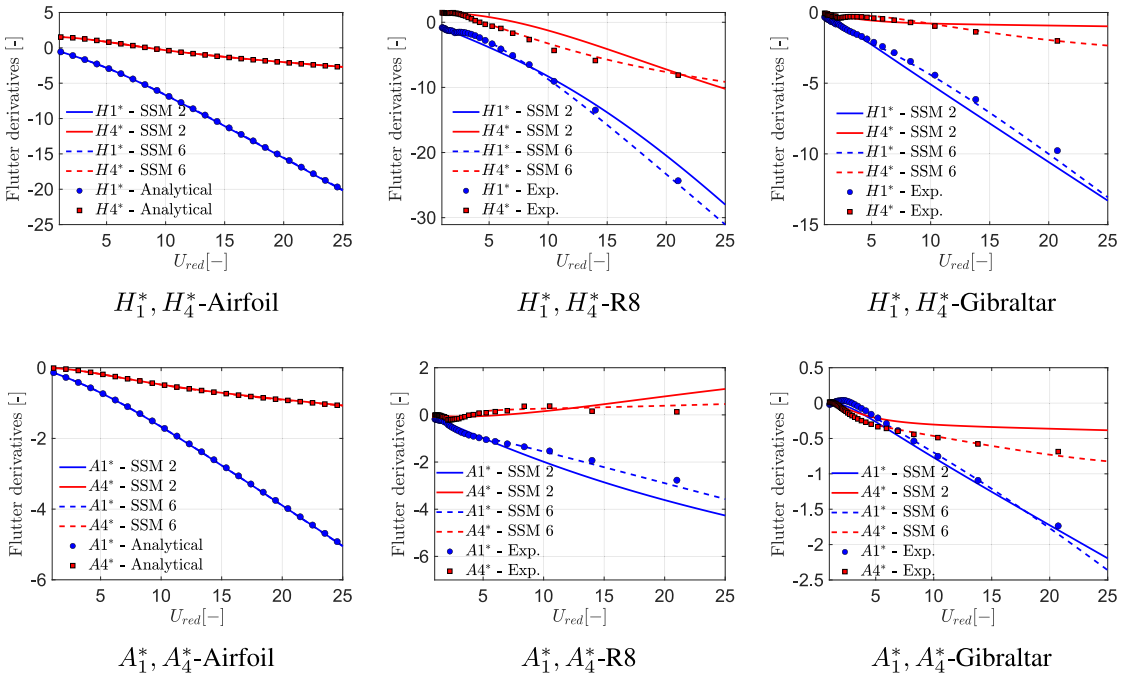


**Fig. 7.** Flutter derivatives related to heaving motion: comparison between target values and SSM results using a variable number of internal states. Markers are experimental values while continuous and dashed lines denote results obtained with the SSM using two and six aerodynamic states, respectively.

states is reported in Figs. 7 and 8. Expectedly, for the thin-airfoil case, the results obtained by the SSM are indistinguishable from the target values, already when two states are considered (the analytical solution is calculated in agreement with the approximate $C(K)$ reported in Eq. (10)). In particular, the two system eigenvalues coincide with the reference values of $-0.091$ and $-0.6$ (up to the tolerances used for the calibration). We notice that, if the regularization terms appearing in Eq. (77) are simply added to $err_H$, then the reference solution cannot be recovered when fitting the model, and the results depends on the value of $\mu_P$ (for instance, if $\mu_P$ is a very large number, the model will tend to minimize $|\boldsymbol{P}|$ rather than minimizing $err_H$). When six states are considered, two of the six eigenvalues are complex, but overall, the model predictions do not change in any substantial way.

Looking at the results obtained for R8 and the Gibraltar Bridge deck, it can clearly be seen that increasing the number of states effectively reduces the differences between the experimental values and those reproduced by the SSM, though two states are often enough to reproduce flutter derivatives fairly well. However, in such a case, the SSM is incapable of accurately reproducing the low $U_{red}$ range, highlighted in the frequency response function reported in Figs. 9 and 10 for the heaving and rotational motion components, respectively.

In general, while for the airfoil monotonic trends are observed, for R8 and the Gibraltar Bridge sections the pattern is more complex, and the SSM is able to reproduce it only when a sufficient number of states is provided. In this regard, however, it shall be recalled that the very low $U_{red}$ range, which is highlighted by the FRF, is often of limited usefulness in applications, and it is also more prone to measurements errors, especially if forced vibrations are used.

Finally, to provide a more complete picture of the results, indicial functions extracted from the calibrated SSM are reported in Fig. 11. In particular, the figure shows the indicial response for both $C_y$ and $C_m$, triggered by step changes in $\alpha$ and $\dot{d}_y$. For the airfoil, as expected, the matching with the approximate Wagner function (see Eq. (5)) is extremely good in all cases. For R8, a clear overshoot of the moment coefficient is visible for both heaving and rotational motion, which is consistent with the presence of the separation bubble at the leading edge. However, the results predicted adopting two and six states are indeed quite consistent despite minor differences. As regard the twin box section, some differences appear when using two or six states, with a slight overshoot with respect to the unitary value occurring only in the second case. In particular, while the response to rotational motion is in reasonable agreement between the two SSMs, heaving

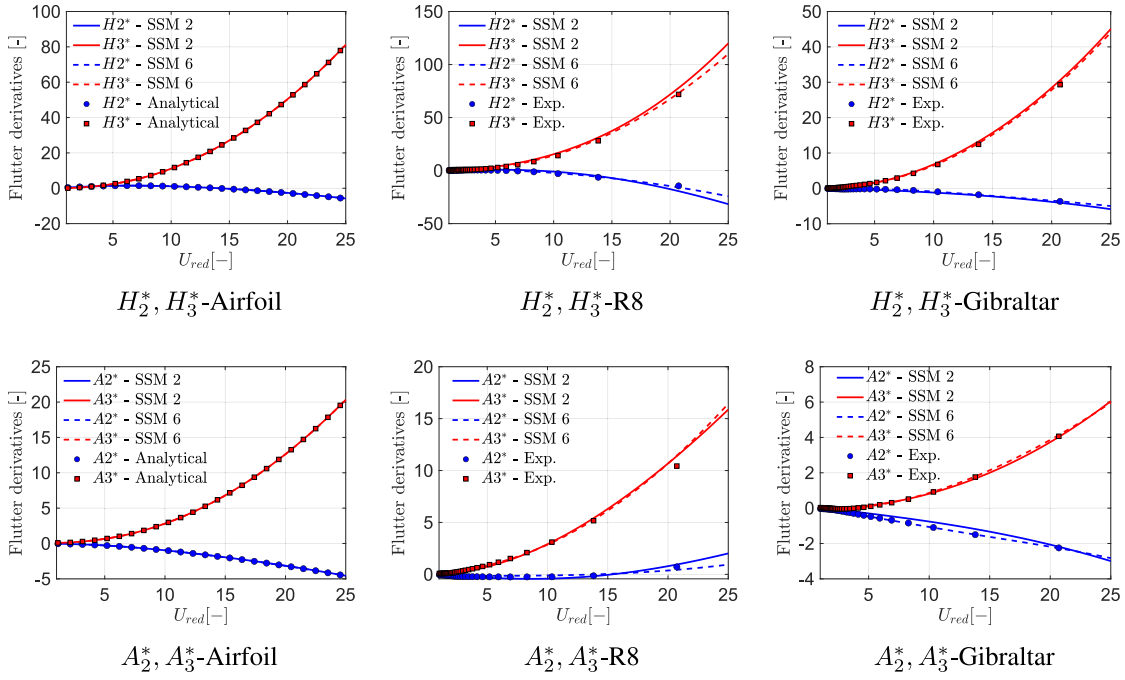


**Fig. 8.** Flutter derivatives related to rotational motion: comparison between target values and SSM results using a variable number of internal states. Markers are experimental values while continuous and dashed lines denote results obtained with the SSM using two and six aerodynamic states, respectively.

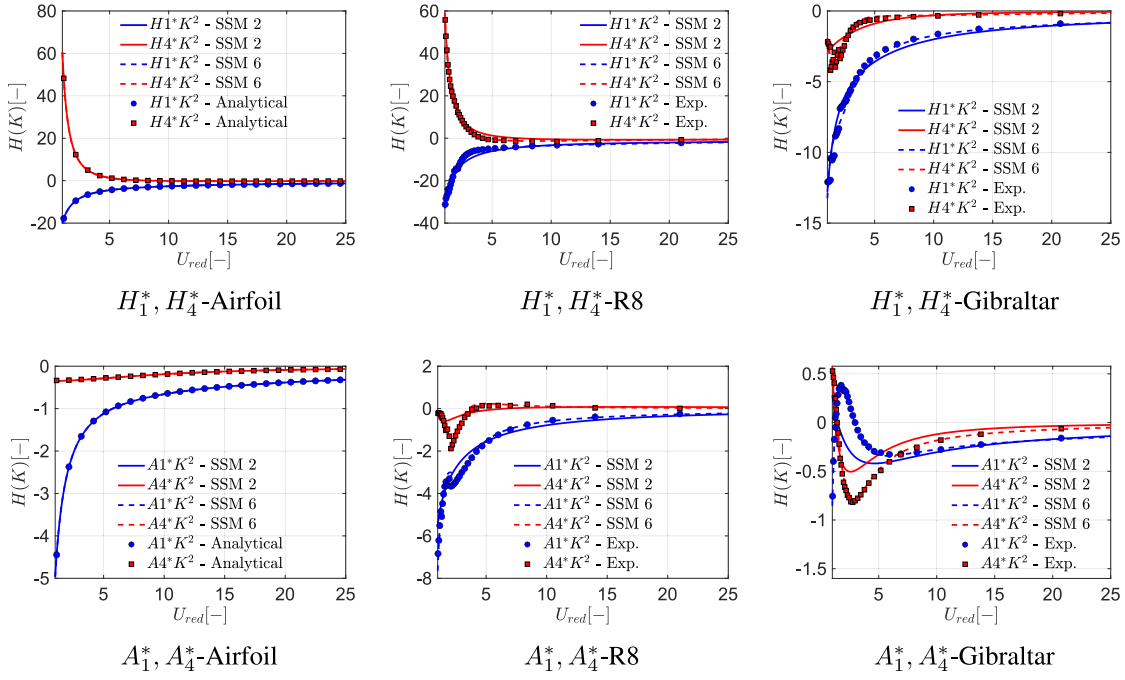


**Fig. 9.** Frequency response function related to heaving motion: comparison between target values and SSM results using a variable number of internal states. Markers are experimental values while continuous and dashed lines denote results obtained with the SSM using two and six aerodynamic states, respectively.

motion triggers an overshoot when six states are considered, which vanishes after approximately 80 nondimensional time units. It is also worth noting that, for the Gibraltar deck section, flutter derivatives $A_1^*$ and $A_4^*$ are visibly better reproduced by the six-states SSM than by the two-states model, corroborating the soundness of the indicial response calculated with six states. Overall, for the considered cases, a SSM comprising four to six states seems to lead to a good reproduction of both flutter derivatives and FRF.

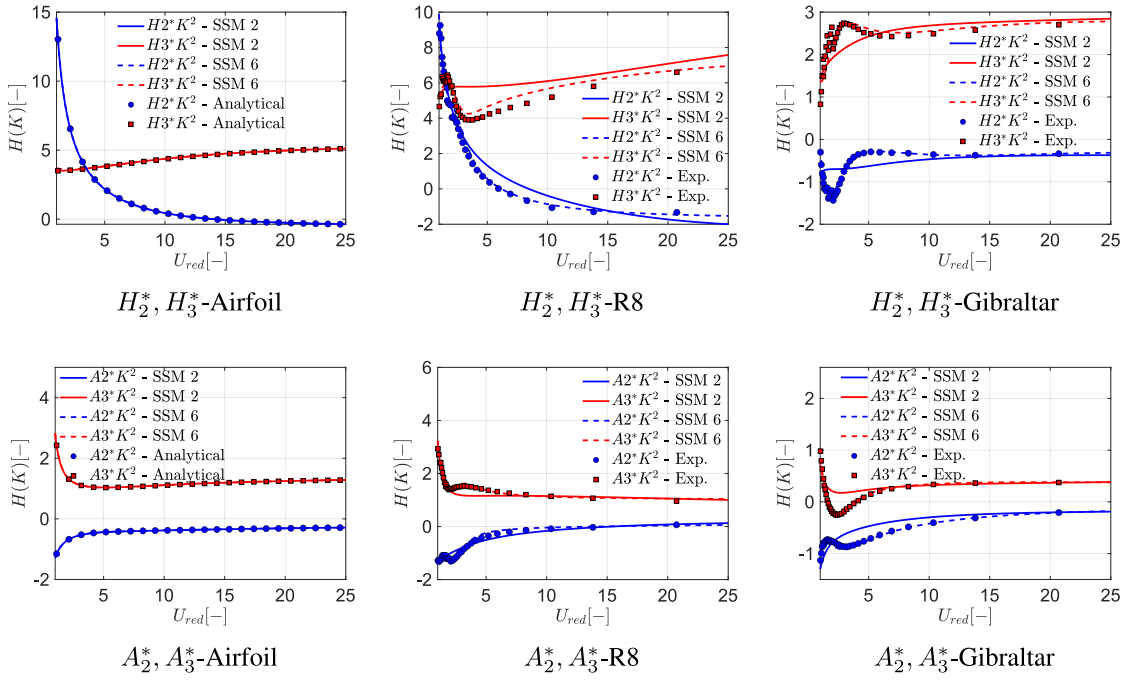


**Fig. 10.** Frequency response function related to rotational motion: comparison between target values and SSM results using a variable number of internal states. Markers are experimental values while continuous and dashed lines denote results obtained with the SSM using two and six aerodynamic states, respectively.

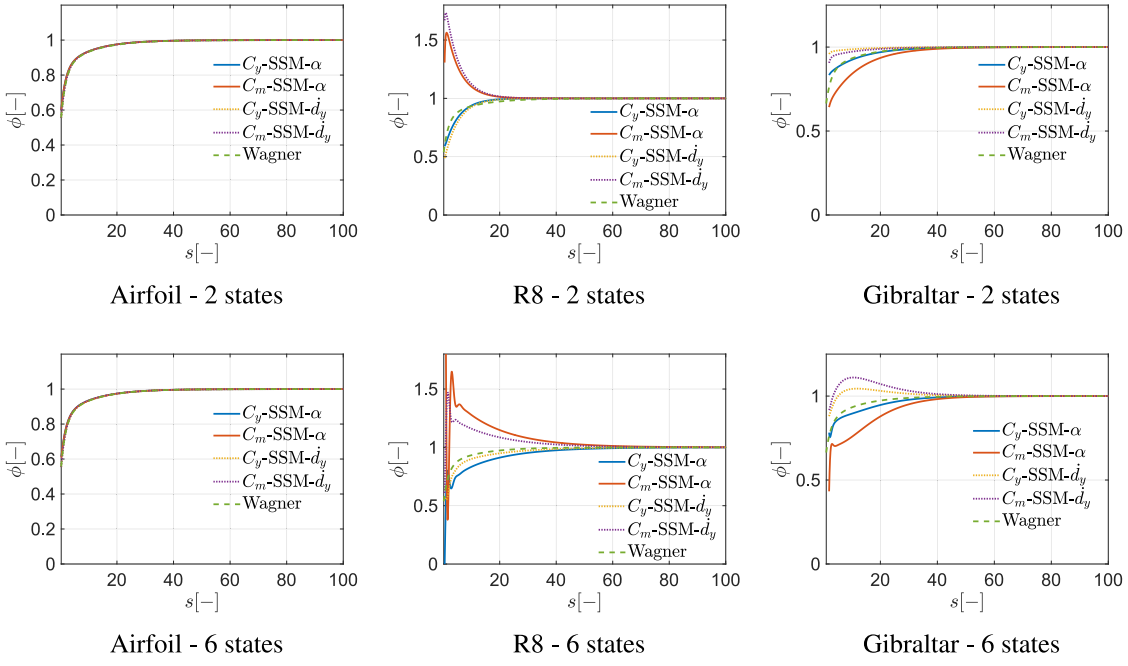


**Fig. 11.** Indicial functions: comparison between results obtained using a variable number of internal states.

### *4.2. Nonlinear model*

We now focus on the nonlinear version of the model, where the model coefficients are expressed as a polynomial expansion with respect to the angle of attack. In this case, we consider two bridge deck sections for which flutter derivatives are available for different mean angles of attack in Barni et al. (2021), namely the Hardanger Bridge section and a twin-box deck section. The geometry and the static coefficients for the two deck sections are reported in Figs. 12 and 13, respectively. For the Hardanger Bridge deck, flutter derivatives were measured in the wind tunnel for various angles of attack between −8° and 8° while, for the twin deck, they were determined for angles of attack between −5° and 5°. The Reader is invited to refer to Barni et al. (2021) for further details regarding the experimental results.

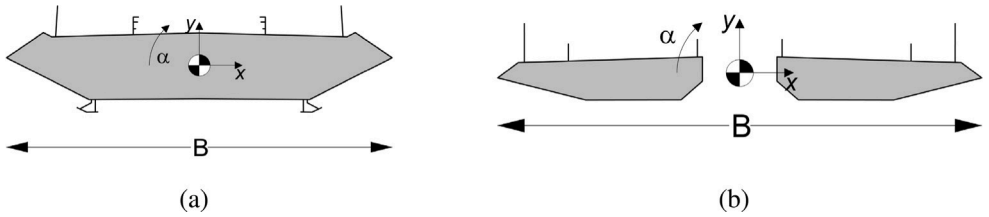


**Fig. 12.** Geometry of the deck sections used for the nonlinear model: (a) Hardanger Bridge and (b) twin-box deck section.

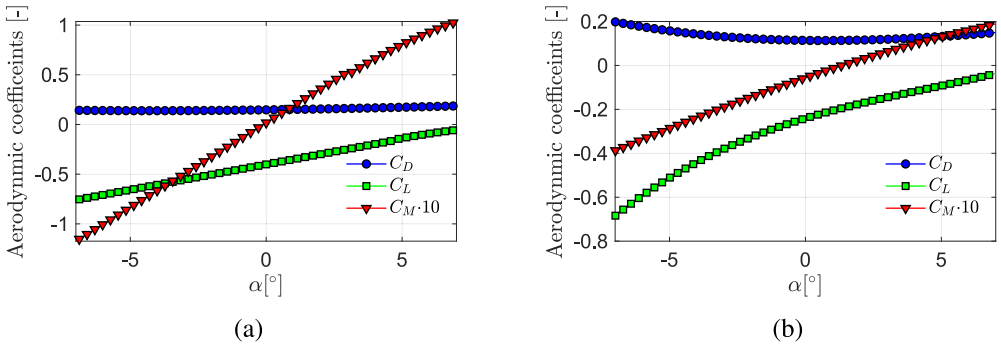


**Fig. 13.** Static aerodynamic coefficients: (a) Hardanger Bridge and (b) twin-box deck section.

For both case studies, we select a total of four aerodynamic states and a quadratic expansion of model matrices' components, leading to a total of 132 model coefficients. Fig. 14 reports the flutter derivatives obtained for the Hardanger Bridge deck, while the results for the twin-box deck section are shown in Fig. 15. It can be seen that in both cases a good agreement is obtained between the experimentally measured flutter derivatives and those reproduced by the SSM, confirming the good performance of the proposed approach.

## 5. Conclusions

In this paper, we investigated the use of State-Space Models, SSM, for the analysis of motion-induced aerodynamic loads on bridge deck sections. Firstly, we introduced a novel SSM formulation, tailored on the structure of airfoil theory, with the aim of providing a simple, yet general, representation of aeroelastic loads. The approach adopts well-established techniques of System and Control Theory, seeking for a minimal, yet clear, parametrization of system behavior. In particular, reversing the point of view usually adopted in the development of similar models, we start by selecting a suitable time-domain formulation of the SSM, ensuring a straightforward applicability of the model if aerodynamic nonlinearities are considered. This leads to the need of carefully separating quasi-static contributions from purely transient terms, so restraining the form assumed by the SSM. Subsequently, the model is linearized, and the corresponding frequency response function is derived, allowing calculating flutter derivatives, which can be used to drive model coefficients' calibration.

The model has been related to similar approaches in the literature and, in particular, to the rational function approximation and to rheological models, providing a comprehensive perspective on the modeling of motion-induced aerodynamic forces by means of SSMs.

The application of the model to the thin-airfoil case and to typical bridge deck sections confirms the good performance of the proposed approach and fitting method.

As a final remark, we notice that the proposed calibration approach exclusively relies on information collected in the frequency domain. While this complies with the usual practice in Wind Engineering, interesting alternatives and/or complementary procedures might arise from the integration of time-domain information, for which a sizable amount of literature in the context of SSM is available.

## CRediT authorship contribution statement

**Simian Lei:** Writing – original draft, Investigation. **Luca Patruno:** Writing – review & editing, Writing – original draft, Methodology, Investigation, Conceptualization. **Claudio Mannini:** Writing – review & editing, Supervision, Methodology. **Stefano de Miranda:** Supervision. **Yaojun Ge:** Supervision.

## Declaration of competing interest

The authors declare that they have no known competing financial interests or personal relationships that could have appeared to influence the work reported in this paper.

## Appendix A

We noticed in Eq. (27) that rotations do not follow the same expression as the other terms. In particular, we can firstly assume rotations to compose according to the usual product rule

$$\boldsymbol{R}(K,s) = \boldsymbol{R}^{\epsilon}(\tilde{\epsilon}e^{iKs})\bar{\boldsymbol{R}}, \tag{A.1}$$

being $\boldsymbol{R}^{\epsilon}(\tilde{\epsilon}e^{iKs})$ the rotation matrix associated with the small fluctuating angle $\tilde{\epsilon}e^{iKs}$, which superimposes with a pre-existing large mean rotation represented by $\bar{\boldsymbol{R}}$. We can approximate $\boldsymbol{R}^{\epsilon}$ to fist order as

$$\boldsymbol{R}^{\epsilon}(K,s) = \boldsymbol{I} + \boldsymbol{J}\tilde{\epsilon}e^{iKs} = \boldsymbol{I} + \tilde{\boldsymbol{R}}e^{iKs}, \tag{A.2}$$

where $\boldsymbol{J}$ is the generator of two-dimensional rotations in the $x$–$y$ plane (clockwise, according to the nose-up convention). In particular, we have

$$\boldsymbol{J} = \begin{bmatrix} 0 & 1 & 0 \\ -1 & 0 & 0 \\ 0 & 0 & 0 \end{bmatrix}, \qquad \tilde{\boldsymbol{R}} = \begin{bmatrix} 0 & \tilde{\epsilon} & 0 \\ -\tilde{\epsilon} & 0 & 0 \\ 0 & 0 & 0 \end{bmatrix}. \tag{A.3}$$

We can thus approximate

$$\boldsymbol{R}(K,s) \approx (\boldsymbol{I} + \tilde{\boldsymbol{R}}e^{iKs})\bar{\boldsymbol{R}} = (\bar{\boldsymbol{R}} + \tilde{\boldsymbol{R}}\bar{\boldsymbol{R}}e^{iKs}). \tag{A.4}$$

The complex amplitude of the aerodynamic forces, $\tilde{\boldsymbol{F}}$, can be calculated substituting Eq. (27) into Eq. (26), yielding

$$\bar{\boldsymbol{F}} + \tilde{\boldsymbol{F}}e^{iKs} = (\bar{q} + \tilde{q}e^{iKs})\boldsymbol{B}(\bar{\boldsymbol{R}} + \tilde{\boldsymbol{R}}\bar{\boldsymbol{R}}e^{iKs})(\bar{\boldsymbol{C}}_a + \tilde{\boldsymbol{C}}_a e^{iKs}). \tag{A.5}$$

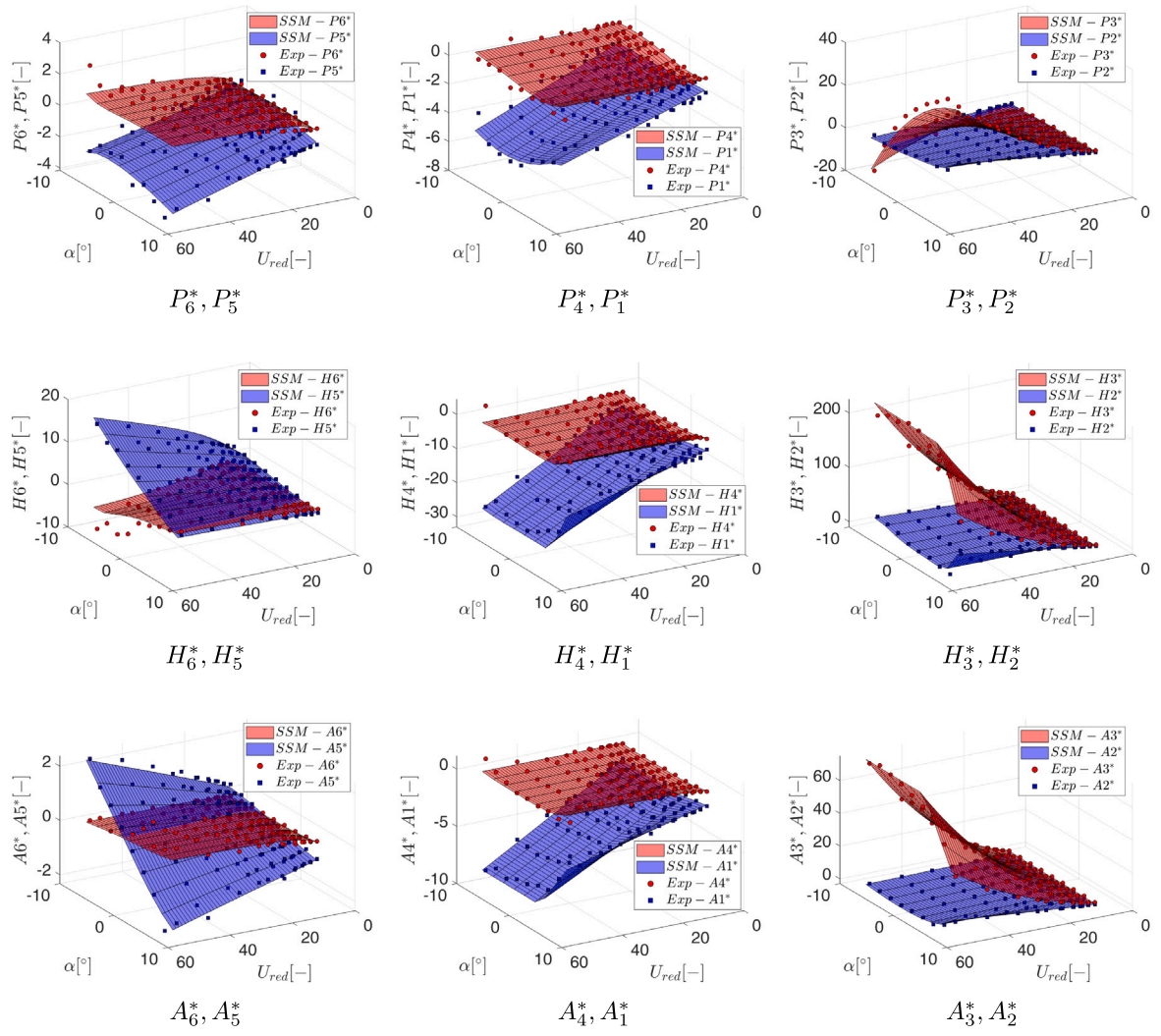


**Fig. 14.** Hardanger Bridge deck flutter derivatives: comparison between measured values and results from the SSM. Markers are the experimental values while surfaces represent the result obtained with the SSM.

Developing the products, we obtain

$$\tilde{\boldsymbol{F}} + \tilde{\boldsymbol{F}}e^{iKs} = \bar{q}\boldsymbol{B}\bar{\boldsymbol{R}}\tilde{\boldsymbol{C}}_a + \bar{q}\boldsymbol{B}\bar{\boldsymbol{R}}\tilde{\boldsymbol{C}}_a e^{iKs} + \bar{q}\boldsymbol{B}\tilde{\boldsymbol{R}}\bar{\boldsymbol{R}}\bar{\boldsymbol{C}}_a e^{iKs} + \bar{q}\boldsymbol{B}\tilde{\boldsymbol{R}}\bar{\boldsymbol{R}}\tilde{\boldsymbol{C}}_a e^{i2Ks} + \tag{A.6}$$

$$\tilde{q}\boldsymbol{B}\bar{\boldsymbol{R}}\bar{\boldsymbol{C}}_a e^{iKs} + \tilde{q}\boldsymbol{B}\bar{\boldsymbol{R}}\tilde{\boldsymbol{C}}_a e^{i2Ks} + \tilde{q}\boldsymbol{B}\tilde{\boldsymbol{R}}\bar{\boldsymbol{R}}\bar{\boldsymbol{C}}_a e^{i2Ks} + \tilde{q}\boldsymbol{B}\tilde{\boldsymbol{R}}\bar{\boldsymbol{R}}\tilde{\boldsymbol{C}}_a e^{i3Ks}. \tag{A.7}$$

The terms containing $e^{i2Ks}$ and $e^{i3Ks}$ can be disregarded as they contain products of small fluctuating quantities. Furthermore, as they derive from nonlinear terms, they are super-harmonics of the excitation. It is thus possible to identify

$$\tilde{\boldsymbol{F}}e^{iKs} = (\bar{q}\boldsymbol{B}\bar{\boldsymbol{R}}\tilde{\boldsymbol{C}}_a + \bar{q}\boldsymbol{B}\tilde{\boldsymbol{R}}\bar{\boldsymbol{R}}\bar{\boldsymbol{C}}_a + \tilde{q}\boldsymbol{B}\bar{\boldsymbol{R}}\bar{\boldsymbol{C}}_a)e^{iKs}, \tag{A.8}$$

which, reordering terms and simplifying the exponential, coincides with Eq. (28).

## Appendix B

We show here that for the proposed model, the FRF reported in Eq. (28) is valid both in the case of constant model matrices and in the more general case in which they depend on the input $\boldsymbol{e}$ and/or $\boldsymbol{C}_a$. Such aspect is of great importance when considering the nonlinear version of the model, in which the coefficients are no more constants.

In particular, we rewrite Eq. (23) as

$$\begin{cases} \dot{\boldsymbol{C}}_r = \boldsymbol{\mathcal{A}}(\boldsymbol{e}, \boldsymbol{C}_a)\boldsymbol{C}_r + \boldsymbol{\mathcal{B}}(\boldsymbol{e}, \boldsymbol{C}_a)\dot{\boldsymbol{e}} \\ \boldsymbol{C}_a = \boldsymbol{C}_a^{eq}(\alpha_e) + \boldsymbol{C}(\boldsymbol{e}, \boldsymbol{C}_a)\boldsymbol{C}_r + \boldsymbol{\mathcal{D}}(\boldsymbol{e}, \boldsymbol{C}_a)\dot{\boldsymbol{e}}. \end{cases} \tag{B.1}$$

We assume small fluctuations in the neighborhood of an equilibrium position:

$$\boldsymbol{e}(K,s) = \tilde{\boldsymbol{e}}e^{iKs}, \qquad \boldsymbol{C}_r(K,s) = \bar{\boldsymbol{C}}_r + \tilde{\boldsymbol{C}}_r e^{iKs}, \qquad \boldsymbol{\mathcal{A}}(K,s) = \bar{\boldsymbol{\mathcal{A}}} + \tilde{\boldsymbol{\mathcal{A}}}e^{iKs}, \tag{B.2}$$

$$\boldsymbol{\mathcal{B}}(K,s) = \bar{\boldsymbol{\mathcal{B}}} + \tilde{\boldsymbol{\mathcal{B}}}e^{iKs}, \qquad \boldsymbol{C}(K,s) = \bar{\boldsymbol{C}} + \tilde{\boldsymbol{C}}e^{iKs}, \qquad \boldsymbol{\mathcal{D}}(K,s) = \bar{\boldsymbol{\mathcal{D}}} + \tilde{\boldsymbol{\mathcal{D}}}e^{iKs}, \tag{B.3}$$

where $\bar{\boldsymbol{e}}$ has been set equal to zero, assuming it to be the reference configuration around which the system oscillates. Substituting the equations above into the first of Eq. (B.1)

$$iK\tilde{\boldsymbol{C}}_r e^{iKs} = [\bar{\boldsymbol{\mathcal{A}}} + \tilde{\boldsymbol{\mathcal{A}}}e^{iKs}][\bar{\boldsymbol{C}}_r + \tilde{\boldsymbol{C}}_r e^{iKs}] + [\bar{\boldsymbol{\mathcal{B}}} + \tilde{\boldsymbol{\mathcal{B}}}e^{iKs}]iK\tilde{\boldsymbol{e}}e^{iKs}. \tag{B.4}$$

Developing the products, we obtain

$$iK\tilde{\boldsymbol{C}}_r e^{iKs} = \bar{\boldsymbol{\mathcal{A}}}\bar{\boldsymbol{C}}_r + \bar{\boldsymbol{\mathcal{A}}}\tilde{\boldsymbol{C}}_r e^{iKs} + \tilde{\boldsymbol{\mathcal{A}}}e^{iKs}\bar{\boldsymbol{C}}_r + \tilde{\boldsymbol{\mathcal{A}}}\tilde{\boldsymbol{C}}_r e^{i2Ks} + iK\bar{\boldsymbol{\mathcal{B}}}\tilde{\boldsymbol{e}}e^{iKs} + iK\tilde{\boldsymbol{\mathcal{B}}}\tilde{\boldsymbol{e}}e^{i2Ks}. \tag{B.5}$$

Removing terms containing products of small fluctuating quantities, we can identify

$$\bar{\boldsymbol{\mathcal{A}}}\bar{\boldsymbol{C}}_r = \boldsymbol{0}, \qquad \tilde{\boldsymbol{C}}_r = \left[iK\boldsymbol{I} - \bar{\boldsymbol{\mathcal{A}}}\right]^{-1} iK\bar{\boldsymbol{\mathcal{B}}}\tilde{\boldsymbol{e}}, \tag{B.6}$$

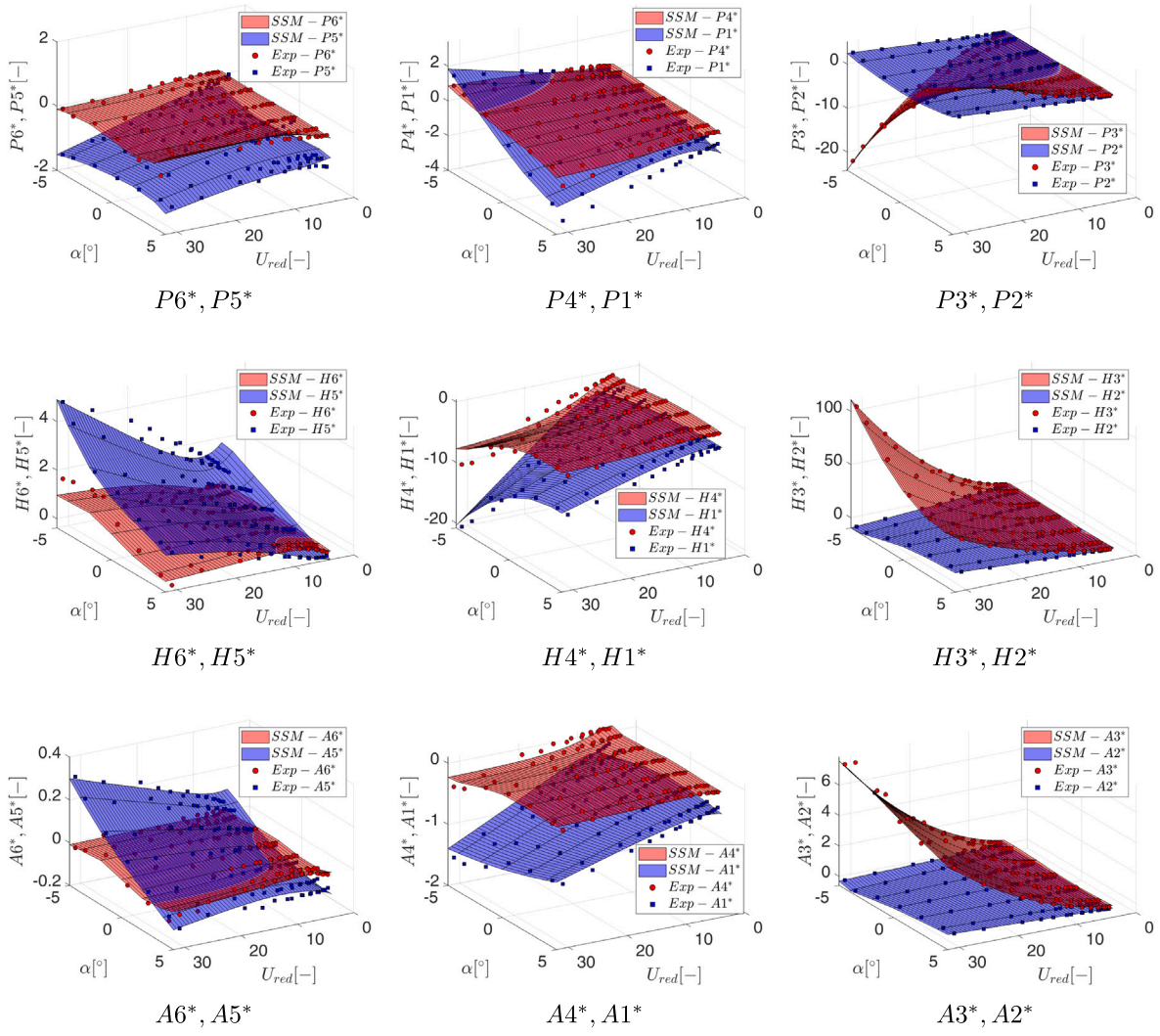


**Fig. 15.** Twin-box bridge deck section flutter derivatives: comparison between measured values and results from the SSM. Markers are the experimental values while surfaces represent the result obtained with the SSM.

where, the first equation, as all eigenvalues of $\bar{\boldsymbol{\mathcal{A}}}$ are strictly positive, implies $\tilde{\boldsymbol{C}}_r = \boldsymbol{0}$, while the second one coincides with Eq. (45), derived for the system characterized by constant matrices. Proceeding analogously for the second of Eq. (B.1), it is possible to conclude that the FRF calculation is not affected by the dependence of model matrices on $\boldsymbol{e}$ and/or $\boldsymbol{C}_a$.

## Appendix C

We now hint at the modifications needed to adopt the $\xi-\eta$ reference system (see Fig. 3), fixed with respect to the section, for the characterization of aerodynamic coefficients. The latters follow the usual transformation between $\xi-\eta$ and $x-y$ reference systems:

$$\boldsymbol{C}_{a,xy} = \boldsymbol{R}\boldsymbol{C}_{a,\xi\eta}, \qquad \boldsymbol{C}_{a,\xi\eta} = \boldsymbol{R}^T\boldsymbol{C}_{a,xy}. \tag{C.1}$$

It is possible to substitute in the first of Eq. (C.1) the relevant expressions with mean and fluctuating quantities (i.e., using Eq. (27)), allowing to identifying

$$\bar{\boldsymbol{C}}_{a,xy} = \bar{\boldsymbol{R}}\bar{\boldsymbol{C}}_{a,\xi\eta}, \tag{C.2}$$

or equivalently, assuming horizontal incoming wind so that $\bar{\boldsymbol{C}}_{a,xy} = \bar{\boldsymbol{C}}_{a,DL} = \boldsymbol{C}^{eq}_{a,DL}$:

$$\boldsymbol{C}^{eq}_{a,DL} = \bar{\boldsymbol{R}}\boldsymbol{C}^{eq}_{a,\xi\eta}. \tag{C.3}$$

With this in mind, we can modify Eq. (22), taking

$$\boldsymbol{R} = \begin{bmatrix} \cos(\alpha(K,s)) & \sin(\alpha(K,s)) & 0 \\ -\sin(\alpha(K,s)) & \cos(\alpha(K,s)) & 0 \\ 0 & 0 & 1 \end{bmatrix}. \tag{C.4}$$

Then, looking at Eq. (A.1) and (A.2), Eq. (37) shall be modified as

$$\bar{\boldsymbol{R}} = \begin{bmatrix} \cos(\bar{\alpha}) & \sin(\bar{\alpha}) & 0 \\ -\sin(\bar{\alpha}) & \cos(\bar{\alpha}) & 0 \\ 0 & 0 & 1 \end{bmatrix}, \qquad \tilde{\boldsymbol{R}} = \begin{bmatrix} 0 & \tilde{\alpha} & 0 \\ -\tilde{\alpha} & 0 & 0 \\ 0 & 0 & 0 \end{bmatrix}, \tag{C.5}$$

which, substituted in Eq. (38), yields

$$\boldsymbol{H}^q = \bar{\boldsymbol{R}}\begin{bmatrix} -2iKC^{eq}_{\xi}(\bar{\alpha}) & 0 & 0 \\ -2iKC^{eq}_{\eta}(\bar{\alpha}) & 0 & 0 \\ -2iKC^{eq}_{M}(\bar{\alpha}) & 0 & 0 \end{bmatrix} = -2iK\begin{bmatrix} C^{eq}_{D}(\bar{\alpha}) & 0 & 0 \\ C^{eq}_{L}(\bar{\alpha}) & 0 & 0 \\ C^{eq}_{M}(\bar{\alpha}) & 0 & 0 \end{bmatrix}, \tag{C.6}$$

where, we recall, it is assumed that the incoming wind is horizontal. Analogously, we can modify Eq. (42) obtaining

$$\boldsymbol{H}^R(K) = \begin{bmatrix} 0 & 0 & C_L^{eq}(\bar{\alpha}) \\ 0 & 0 & -C_D^{eq}(\bar{\alpha}) \\ 0 & 0 & 0 \end{bmatrix}. \tag{C.7}$$

As regard $\boldsymbol{H}^C(K)$, we have to modify Eq. (49) as

$$\boldsymbol{H}^C(K) = \bar{\boldsymbol{R}} \left\{ \boldsymbol{C}'_{a,\xi\eta} \frac{\mathrm{d}\alpha_e}{\mathrm{d}e} + \boldsymbol{C} \left[ iK\boldsymbol{I} - \boldsymbol{\mathcal{A}} \right]^{-1} iK\boldsymbol{\mathcal{B}} + iK\boldsymbol{\mathcal{D}} \right\} \boldsymbol{T}(K), \tag{C.8}$$

in which we remind that the prime indicates a derivative with respect to the angle of attack. Taking the derivative of both sides of Eq. (C.2) with respect to $\bar{\alpha}$ and, remembering that aerodynamic coefficients with an overline indicate equilibrium coefficients, we have

$$\boldsymbol{C}'_{a,xy} = \bar{\boldsymbol{R}}' \boldsymbol{C}^{eq}_{a,\xi\eta} + \bar{\boldsymbol{R}} \boldsymbol{C}'_{a,\xi\eta} = \boldsymbol{J}\bar{\boldsymbol{R}} \boldsymbol{C}^{eq}_{a,\xi\eta} + \bar{\boldsymbol{R}} \boldsymbol{C}'_{a,\xi\eta}, \tag{C.9}$$

where the chain rule of derivation was used and $\boldsymbol{R}'$, the derivative of the rotation matrix with respect to the angle, was expressed using the generator of $2D$ rotations (see Eq. (A.3)). Rearranging terms, we obtain

$$\bar{\boldsymbol{R}} \boldsymbol{C}'_{a,\xi\eta} = \boldsymbol{C}'_{a,xy} - \boldsymbol{J}\bar{\boldsymbol{R}} \boldsymbol{C}^{eq}_{a,\xi\eta} = \boldsymbol{C}'_{a,DL} - \boldsymbol{J}\boldsymbol{C}^{eq}_{a,DL}, \tag{C.10}$$

in which, once again, we used that $\boldsymbol{C}^{eq}_{a,xy} = \boldsymbol{C}^{eq}_{a,DL}$. We can thus rewrite Eq. (C.8) as

$$\begin{aligned} \boldsymbol{H}^C(K) = \left[ \boldsymbol{C}'_{a,DL} - \boldsymbol{J}\boldsymbol{C}^{eq}_{a,DL}(\bar{\alpha}) \right] \frac{\mathrm{d}\alpha_e}{\mathrm{d}e} \boldsymbol{T}(K) + \bar{\boldsymbol{R}} \Big\{ \boldsymbol{C} \left[ iK\boldsymbol{I} - \boldsymbol{\mathcal{A}} \right]^{-1} iK\boldsymbol{\mathcal{B}} \\ + iK\boldsymbol{\mathcal{D}} \Big\} \boldsymbol{T}(K), \end{aligned} \tag{C.11}$$

where it can be noticed that some differences appear compared to the expression provided in Eq. (49). We can develop the first addendum in Eq. (C.11) as

$$\begin{aligned} &\left[ \boldsymbol{C}'_{a,DL} - \boldsymbol{J}\boldsymbol{C}^{eq}_{a,DL}(\bar{\alpha}) \right] \frac{\mathrm{d}\alpha_e}{\mathrm{d}e} \boldsymbol{T}(K) \\ &= \begin{bmatrix} 0 & -[C'_D - C_L^{eq}(\bar{\alpha})]iK & [C'_D - C_L^{eq}(\bar{\alpha})] \\ 0 & -[C'_L + C_D^{eq}(\bar{\alpha})]iK & [C'_L + C_D^{eq}(\bar{\alpha})] \\ 0 & -iKC'_M & C'_M \end{bmatrix}, \end{aligned} \tag{C.12}$$

noticing that this is the only contribution to $\boldsymbol{H}^C(K)$ in the quasi-static limit. Summing also the contributions from $\boldsymbol{H}^q$ and $\boldsymbol{H}^R$, we obtain the quasi-static $\boldsymbol{H}^{qs}(K)$ as

$$\boldsymbol{H}^{qs}(K) = \begin{bmatrix} -iK2C_D^{eq}(\bar{\alpha}) & -iK[C'_D - C_L^{eq}(\bar{\alpha})] & C'_D \\ -iK2C_L^{eq}(\bar{\alpha}) & -iK[C'_L + C_D^{eq}(\bar{\alpha})] & C'_L \\ -iK2C_M^{eq}(\bar{\alpha}) & -iKC'_M & C'_M \end{bmatrix}, \tag{C.13}$$

which coincides with the expression provided in Section 3.1.4. It can thus be concluded that, as expected, formulating the model assuming that the aerodynamic coefficients are expressed either in the wind or in the section reference system is completely equivalent for the quasi-static response. However, a difference arises in the contributions of aerodynamic states and bypass term, namely in the second addendum of Eq. (C.11) when $\bar{\boldsymbol{R}} \neq \boldsymbol{I}$.

## Appendix D

We now demonstrate that the proposed model, in which $\dot{\boldsymbol{e}}$ appears as forcing term, is actually equivalent to a model with the same form, but where $\boldsymbol{e}$ appears instead. Starting from the linearized version of the proposed model, which reads

$$\begin{cases} \dot{\boldsymbol{C}}_r = \boldsymbol{\mathcal{A}}\boldsymbol{C}_r + \boldsymbol{\mathcal{B}}\dot{\boldsymbol{e}}, \\ \boldsymbol{C}_a = \boldsymbol{C}'_a \frac{\mathrm{d}\alpha_e}{\mathrm{d}e} \boldsymbol{e} + \boldsymbol{C}\boldsymbol{C}_r + \boldsymbol{\mathcal{D}}\dot{\boldsymbol{e}}, \end{cases} \tag{D.1}$$

the second equation can be rewritten as

$$\boldsymbol{C}_a = \boldsymbol{C}\boldsymbol{C}_r + \boldsymbol{\mathcal{E}}\boldsymbol{e} + \boldsymbol{\mathcal{D}}\dot{\boldsymbol{e}}, \tag{D.2}$$

being $\boldsymbol{\mathcal{E}} = \boldsymbol{C}'_a \frac{\mathrm{d}\alpha_e}{\mathrm{d}e}$ the term accounting for the quasi-static response. Let us consider a new set of aerodynamic states such that

$$\boldsymbol{C}_t = \boldsymbol{C}_r - \boldsymbol{\mathcal{B}}\boldsymbol{e}; \tag{D.3}$$

then, upon derivation,

$$\dot{\boldsymbol{C}}_t = \dot{\boldsymbol{C}}_r - \boldsymbol{\mathcal{B}}\dot{\boldsymbol{e}}. \tag{D.4}$$

Extracting $\boldsymbol{C}_r$ and $\dot{\boldsymbol{C}}_r$ from Eqs. (D.3) and (D.4), we can rewrite Eq. (D.2) as

$$\begin{cases} \dot{\boldsymbol{C}}_t = \boldsymbol{\mathcal{A}}\boldsymbol{C}_t + \boldsymbol{\mathcal{A}}\boldsymbol{\mathcal{B}}\boldsymbol{e}, \\ \boldsymbol{C}_a = \boldsymbol{C}\boldsymbol{C}_t + (\boldsymbol{C}\boldsymbol{\mathcal{B}} + \boldsymbol{\mathcal{E}})\boldsymbol{e} + \boldsymbol{\mathcal{D}}\dot{\boldsymbol{e}}, \end{cases} \tag{D.5}$$

in which the forcing term of the aerodynamic states is now represented by $\boldsymbol{e}$. It is thus shown that the proposed model, in which the forcing term is represented by $\dot{\boldsymbol{e}}$, is equivalent to the version in which the forcing term is $\boldsymbol{e}$. The only difference is that in the second case, some quasi-static contributions are entangled with the aerodynamic states.

Analogously, defining a new set of aerodynamic states such that

$$\boldsymbol{C}_s = \boldsymbol{C}_r + \boldsymbol{\mathcal{A}}^{-1}\boldsymbol{\mathcal{B}}\dot{\boldsymbol{e}}, \tag{D.6}$$

the system of Eqs. (D.1) might be rewritten as

$$\begin{cases} \dot{\boldsymbol{C}}_s = \boldsymbol{\mathcal{A}}\boldsymbol{C}_s + \boldsymbol{\mathcal{A}}^{-1}\boldsymbol{\mathcal{B}}\ddot{\boldsymbol{e}}, \\ \boldsymbol{C}_a = \boldsymbol{C}\boldsymbol{C}_s + \boldsymbol{\mathcal{E}}\boldsymbol{e} + (\boldsymbol{\mathcal{D}} - \boldsymbol{C}\boldsymbol{\mathcal{A}}^{-1}\boldsymbol{\mathcal{B}})\dot{\boldsymbol{e}}, \end{cases} \tag{D.7}$$

in which the aerodynamic states are now forced by $\ddot{\boldsymbol{e}}$. This shows that the order of the derivatives occurring in the forcing of the aerodynamic states can be changed upon an appropriate modification of the other terms defining the SSM. The same line of reasoning can be used to demonstrate that the classical RFA model, in which $\dot{\boldsymbol{w}}$ represents the forcing term, is equivalent to that in which $\ddot{\boldsymbol{w}}$ is used instead.

## Data availability

Data will be made available on request.

## References


Barni, N., Bartoli, G., Mannini, C., 2024. Lyapunov stability of suspension bridges in turbulent flow. Nonlinear Dynam. 112 (19), 16711–16732.

Barni, N., Mannini, C., 2024. Parametric effects of turbulence on the flutter stability of suspension bridges. J. Wind Eng. Ind. Aerodyn. 245, 105615.

Barni, N., Øiseth, O., Mannini, C., 2021. Time-variant self-excited force model based on 2D rational function approximation. J. Wind Eng. Ind. Aerodyn. 211, 104523.

Barni, N., Øiseth, O.A., Mannini, C., 2022. Buffeting response of a suspension bridge based on the 2D rational function approximation model for self-excited forces. Eng. Struct. 261, 114267.

Barni, N., Øiseth, O.A., Mannini, C., 2023. Nonlinear buffeting response of long suspension bridges considering parametric excitation due to large-scale turbulence. In: IABSE Symposium Istanbul 2023: Long Span Bridges - Proceeding Book. pp. 351–358.

Calamelli, F., Rossi, R., Argentini, T., Rocchi, D., Diana, G., 2024. A nonlinear approach for the simulation of the buffeting response of long span bridges under non-synoptic storm winds. J. Wind Eng. Ind. Aerodyn. 247, 105681.

Caracoglia, L., Jones, N.P., 2003. Time domain vs. frequency domain characterization of aeroelastic forces for bridge deck sections. J. Wind Eng. Ind. Aerodyn. 91 (3), 371–402.

Chen, X., Kareem, A., 2001. Nonlinear response analysis of long-span bridges under turbulent winds. J. Wind Eng. Ind. Aerodyn. 89, 1335–1350.

Chen, X., Kareem, A., 2003. Aeroelastic analysis of bridges: effects of turbulence and aerodynamic nonlinearities. J. Eng. Mech. 129 (8), 885–895.

Chen, X., Matsumoto, M., Kareem, A., 2000a. Aerodynamic coupling effects on flutter and buffeting of bridges. J. Eng. Mech. 126, 17–26.

Chen, X., Matsumoto, M., Kareem, A., 2000b. Time domain flutter and buffeting response analysis of bridges. J. Eng. Mech. 126, 7–16.

De Schutter, B., 2000. Minimal state-space realization in linear system theory: an overview. Int. J. Comput. Appl. Math. 121 (1–2), 331–354.

Diana, G., Bruni, S., Cigada, A., Collina, A., 1993. Turbulence effect on flutter velocity in long span suspended bridges. J. Wind Eng. Ind. Aerodyn. 48, 329–342.

Diana, G., Omarini, S., 2020. A non-linear method to compute the buffeting response of a bridge validation of the model through wind tunnel tests. J. Wind Eng. Ind. Aerodyn. 201, 104163.

Diana, G., Resta, F., Rocchi, D., 2008. A new numerical approach to reproduce bridge aerodynamic non-linearities in time domain. J. Wind Eng. Ind. Aerodyn. 96, 1871–1884.
Diana, G., Rocchi, D., Argentini, T., 2013. An experimental validation of a band superposition model of the aerodynamic forces acting on multi-box deck sections. J. Wind Eng. Ind. Aerodyn. 113, 40–58.
Diana, G., Rocchi, D., Argentini, T., Muggiasca, S., 2010. Aerodynamic instability of a bridge deck section model: Linear and nonlinear approach to force modeling. J. Wind Eng. Ind. Aerodyn. 98, 363–374.
Diana, G., Stoyanoff, S., Allsop, A., Amerio, L., Andersen, M.S., Argentini, T., Calamelli, F., Montoya, M.C., de Goyet, V.d., Hernandez, S., 2023. IABSE task group 3.1 benchmark results. Numerical full bridge stability and buffeting simulations. Struct. Eng. Int. 33, 623–634.
Friedland, B., 2012. Control System Design: an Introduction to State-Space Methods. Courier Corporation.
Fung, Y.C., 2008. An introduction to the theory of aeroelasticity. Courier Dover Publications.
Gao, G., Zhu, L., Li, J., Han, W., 2020. Application of a new empirical model of nonlinear self-excited force to torsional vortex-induced vibration and nonlinear flutter of bluff bridge sections. J. Wind Eng. Ind. Aerodyn. 205, 104313.
Garrick, I.E., 1938. On Some Reciprocal Relations in the Theory of Nonstationary Flows. Report 629, pp. 347–350.
Jones, R.T., 1940. The Unsteady Lift of a Wing of Finite Aspect Ratio. Vol. 681.
Král, R., Pospíšil, S., Náprstek, J., 2014. Wind tunnel experiments on unstable self-excited vibration of sectional girders. J. Fluids Struct. 44, 235–250.
Leishman, J.G., 2002. Challenges in modelling the unsteady aerodynamics of wind turbines. Wind Energy 5 (2–3), 85–132.
McKelvey, T., Helmersson, A., 1996. State-space parametrizations of multivariable linear systems using tridiagonal matrix forms. In: Proceedings of 35th IEEE Conference on Decision and Control. Vol. 4, IEEE, pp. 3654–3659.
Müller, A.C., Guido, S., 2016. Introduction to Machine Learning with Python: a Guide for Data Scientists. "O'Reilly Media, Inc.".
Náprstek, J., Pospíšil, S., Hračov, S., 2007. Analytical and experimental modelling of non-linear aeroelastic effects on prismatic bodies. J. Wind Eng. Ind. Aerodyn. 95 (9–11), 1315–1328.
Øiseth, O., Rönnquist, A., Sigbjörnsson, R., 2011. Time domain modeling of self-excited aerodynamic forces for cable-supported bridges: A comparative study. Comput. Struct. 89 (13–14), 1306–1322.
Pospíšil, S., Náprstek, J., Hračov, S., 2006. Stability domains in flow–structure interaction and influence of random noises. J. Wind Eng. Ind. Aerodyn. 94 (11), 883–893.
Roger, K.L., 1977. Airplane math modeling methods for active control design.
Scanlan, R.H., 1993. Problematics in formulation of wind-force models for bridge decks. J. Eng. Mech. 119, 1353–1375.
Sears, W.R., 1941. Some aspects of non-stationary airfoil theory and its practical application. J. Aeronaut. Sci. 8, 104–108.
Starossek, U., Aslan, H., Thiesemann, L., 2009. Experimental and numerical identification of flutter derivatives for nine bridge deck sections. Wind Struct. 12 (6), 519.
Taha, H.E., Rezaei, A.S., 2020. On the high-frequency response of unsteady lift and circulation: A dynamical systems perspective. J. Fluids Struct. 93, 102868.
Theodorsen, T., 1949. General theory of aerodynamic instability and the mechanism of flutter.
Van Oudheusden, B., 1995. On the quasi-steady analysis of one-degree-of-freedom galloping with combined translational and rotational effects. Nonlinear Dynam. 8, 435–451.
Wagner, H., 1924. Über die entstehung des dynamischen auftriebes von tragflügeln.
Wu, T., Kareem, A., 2011. Modeling hysteretic nonlinear behavior of bridge aerodynamics via cellular automata nested neural network. J. Wind Eng. Ind. Aerodyn. 99 (4), 378–388.
Wu, T., Kareem, A., 2013. Bridge aerodynamics and aeroelasticity: A comparison of modeling schemes. J. Fluids Struct. 43, 347–370.
Wu, T., Kareem, A., 2014. Simulation of nonlinear bridge aerodynamics: A sparse third-order Volterra model. J. Sound Vib. 333 (1), 178–188.
Zhou, R., Ge, Y., Yang, Y., Du, Y., Zhang, L., 2018. Wind-induced nonlinear behaviors of twin-box girder bridges with various aerodynamic shapes. Nonlinear Dynam. 94, 1095–1115.